C.P. No. 1307

C.P. No. 1307

PROCUREMENT EXECUTIVE, MINISTRY OF DEFENCE

AERONAUTICAL RESEARCH COUNCIL

CURRENT PAPERS

The Prediction of Boundary-Layer Behaviour and Profile Drag for Infinite Yawed Wings:

Part 1 A Method of Calculation

by

B. G. J. Thompson and A. G. J. Macdonald

Aerodynamics Dept., R.A.E., Teddington

LONDON: HER MAJESTY'S STATIONERY OFFICE

1974

PRICE £1 - 55 NET

UDC 533.693.1 : 532.526 : 532.526.2 : 532.526.4 : 533.6.013.122 : 533.6.013.154

* CP No.1307
May 1973

THE PREDICTION OF BOUNDARY-LAYER BEHAVIOUR AND PROFILE DRAG FOR INFINITE YAWED WINGS:

Part I A METHOD OF CALCULATION

by

B. G. J. Thompson**
A. G. J. Macdonald

SUMMARY

Cumpsty and Head's entrainment method for turbulent boundary layers is extended to compressible flow using Green's compressibility assumptions. The laminar layer is predicted using Thwaites' method in the chordwise plane and the Nath method spanwise. The Rott compressibility transformation is used. The transition and wake assumptions are consistent with the two-dimensional profile drag method of Nash.

The complete method, suitable for use in making routine design calculations, is described briefly. The relationships between calculation time, step length and accuracy are considered for a practical infinite wing at transonic cruise conditions.

The global iteration technique adopted earlier by Cumpsty and Head is shown to fail in regions of favourable pressure gradient, just downstream of the leading edge, as 'correction' terms involving derivatives of integral cross-flow thicknesses are no longer small. A much faster step-by-step numerical method has been adopted to solve the differential equations of the integral turbulent boundary-layer method without convergence problems.

---

* Replaces RAE Technical Report 73092 - ARC 35096

** Now with the DOE, CEDAR Project, PCAO(DBD), Lunar House, Croydon

CONTENTS

1 INTRODUCTION

The present Report initiates a series of three papers concerned with making predictions of the characteristics of viscous flow about infinite yawed wings.

Part III[1] gives the results of a parametric study for a particular infinite wing having a chordwise section (normal to its generators) of RAE (NPL) 3111, operating at its design flat rooftop condition. Profile drag, displacement effect and rear separation behaviour are each considered and the influence of sweep and of Reynolds number presented in chart form. A simple project analysis for an idealised variable sweep wing is used to demonstrate the practical usefulness of the calculated results

Part II[2] shows that current turbulent boundary-layer methods encounter difficulties when attempting to predict the flow in the region of strong favourable pressure gradient just downstream of the swept attachment line. This can lead to uncertainties in the prediction of boundary-layer properties, at the position of a leading-edge velocity peak (say), that might be large enough to lead to serious errors in the subsequent boundary-layer prediction in the adverse pressure gradient flow downstream. Further, it is shown that problems could arise due to the possibility of reversion to laminar flow, in the favourable pressure gradient region, even under flight conditions. Estimates of the uncertainty in drag prediction due to this additional cause are made and it is shown that they could reach several per cent of the value of the upper surface profile drag. Charts are presented enabling a swept wing with a cylindrical leading edge to be designed to investigate further these problems in the wind tunnel.

The basis of the foregoing work, involving some hundreds of boundary-layer calculations, is the complete prediction method now to be described in the present paper. This method employs some simple numerical techniques to handle the input pressure distributions and the aerofoil ordinates neither of which are usually smooth. The data do not have to be at special input spacings (e.g. at the Weber stations or at equal intervals of x'/c'). The description of this numerical work is given in section 2.1.

The subsequent sections describe the compressible laminar boundary-layer calculations which uses the methods of Thwaites[3] chordwise and Nath[4] spanwise. The Rott[5] compressibility transformation is applied.

The assumptions for transition follow closely the ideas of Cooke[6] and of Nash[13] (see section 2.2.2).

If the flow is turbulent at the attachment line, an extension of Cumpsty and Head's[8] treatment for incompressible flow is used up to $M_{a.l.} = 2$.

The turbulent boundary layer (see section 2.3) is then predicted by means of the entrainment method[9,10] extended to compressible flow using the mean velocity profile and skin-friction assumptions due to Green[11,12]. Finally, the turbulent wake is calculated, and values of profile drag found also, by a treatment similar to that of Cooke[6]. However, the chordwise solution in the wake is modified to be compatible with the work of Nash[13,34] in two-dimensions as the latter has been used frequently, in this country, to predict the profile drag of aerofoils.

The numerical solution of the turbulent boundary layer equations uses a simple, fast, step-by-step procedure instead of the original global iteration scheme proposed by Cumpsty and Head[9]. This latter method is shown to diverge uncontrollably in favourable pressure gradients immediately downstream of the leading edge attachment line.

Further numerical results (see section 3), of interest to the practical user of the method, are given for a severe design case having strong rear loading and a mild shock wave present at the flight conditions:

$$\Lambda = 30^{\circ}, \quad M_{\infty} \cos \Lambda = 0.76, \quad Re = 40 \times 10^{6} \quad .$$

These conditions would be typical of an advanced transonic transport aircraft.

It is concluded that, whilst the physical assumptions of the present method leave something to be desired, it remains the only available user-oriented method for design application in compressible flow across the complete chord of the wing. The turbulence energy method[14] as programmed cannot be used close to the swept attachment line. This latter method predicts a variation of rear separation position, with angle of yaw, that is different from the present method but, when expressed in terms of the local boundary-layer thickness, these differences are very small.

As far as predicting exchange rates, between quantities of practical importance, is concerned it is more important to gain experience with the

present crude method than to await the nominally better methods of the future. The comparative success of the simple entrainment method[15] in two-dimensional flow lends strong support to this philosophy.

2 THE CALCULATION METHOD

2.1 Numerical treatment of input ordinates and of the properties of the potential flow

2.1.1 Calculation of surface distance

The aerofoil section shape $z/c'(x'/c')$ normal to the generators of the wing is assumed to have the form

$$z' \propto \sqrt{x'} \quad , \tag{1}$$

close to the leading edge and extra detail is obtained by linear interpolation between ordinates supplied at reasonably closely spaced intervals (e.g. as required for the manufacture of a wind tunnel model).

Surface distance (s'/c'), from the attachment line in this chordwise plane, is then calculated from Pythagoras' theorem assuming the surface to be made up of linear segments between the successive ordinates $z'(x')$.

2.1.2 The treatment of the external velocity distribution close to the leading edge

(a) The choice of step length for laminar boundary layer calculations if there is a sharp leading edge velocity peak

The laminar calculation (see section 2.2 later) is usually carried out on intervals of $\Delta s' = 0.01c'$. However if there are rapid changes in velocity gradient $\left(d(U_1/U_{1_\infty})/d(s'/c')\right)$ close to the leading edge, as for example shown schematically in Fig.1, where there is a sharp peak in velocity close to the attachment line, a shorter step size is selected by the program such that there are 20 equal steps in s'/c' across the (rounded) distance $(2s'_p/c')$ where s'_p is the distance from attachment line to velocity maximum.

(b) Determination of velocity gradient close to the attachment line

From experience, the authors found that most measured pressure distributions are lacking in detail and (usually) are not smooth near to the attachment line.

Figs.2a, 2b and 2c show possible situations in terms of the distributions of associated values of $U_1/U_{1_\infty}(s'/c')$. The first three values are inspected

by the program and, if truly 'scattered', as in Fig.2a, the first point (a) is reset as shown. If the mean slopes from the origin to the points (a), (b) and (c) vary monotonically as in Figs.2b or 2c, then, if the magnitudes of these slopes differ by more than 20% between successive values, point (a) is again adjusted as indicated in the figures.

The value of velocity gradient $\left(d(U_l/U_{l_\infty})/d(s'/c')\right)$ required to start the turbulent calculation is then calculated from the mean slope using the smoothed first point (a).

(c) Velocity gradients at any general position along the chord

Quadratic curves are fitted through three successive $(U_l/U_{l_\infty}, s'/c')$ points at a time and the slopes at the middle points are evaluated and stored. Linear interpolation, on these stored values, to intermediate positions ensures continuity of velocity gradient everywhere across the chord.

2.2 Laminar attachment line flow

2.2.1 The laminar boundary-layer calculation method

(a) The principle of independence in compressible flow

Nath[4] showed how the independence principle can be applied together with the assumption of a universal spanwise velocity profile to solve approximately the laminar boundary-layer equations in their integral momentum form for compressible flow. He used the compressibility transformation due to Stewartson[16]. In the present work a similar approach is employed which adopts the Pohlhausen quartic velocity profiles for the chordwise flow and the zero pressure gradient member* of that family for the spanwise flow. The compressibility transformation due to Rott[5] is used and so the results reduce to those of Nash[7] in two-dimensional conditions.

Provided the condition (see Nath[4]) that

$$L = \frac{\frac{1}{2}(\gamma - 1)M_\infty^2}{1 + \left\{1 + \frac{1}{2}(\gamma - 1)M_\infty^2\right\}\cot^2 \Lambda} \ll 1 \quad , \qquad (2)$$

is satisfied, then the chordwise and the spanwise solutions can be satisfactorily uncoupled. For $\Lambda = 30^\circ$, even with an advanced practical aerofoil section (cruising at $M_\infty \cos \Lambda = 0.8$, say) this seems to be an adequate assumption, since then $L = 0.038$.

However, if the sweep were to rise to 60°, the value of L rises to 0.3 and so it is possible that the independence principle leads to significant errors for sweep angles greater than about 45°.

(b) The chordwise solution

In incompressible flow, Thwaites' solution[3] for the chordwise momentum growth takes the form,

$$\left(\theta_{x_i}\right)^2 = \frac{0.45\nu_i}{U_{1_i}^6} \int_{s_i'}^{s'} U_{1_i}^5 \, ds' \quad . \tag{3}$$

Assuming a recovery factor of $r = 0.85$, a laminar Prandtl number $Pr_1 = 0.72$ and a viscosity/temperature index $n = 0.76$, we find, by applying the Rott transformation with partial stagnation line conditions as reference*, that equation (3) becomes:

$$\left(\frac{\theta_x}{c'}\right)^2 = \frac{0.45}{R_{c'}} \frac{1}{\left(\frac{U_1}{U_{1_\infty}}\right)^6} \left(\frac{T_0}{T_e}\right)^{3.3} \left(\frac{T_\infty}{T_0}\right)^{1.74} \int_{\frac{s'}{c'}} \left(\frac{U_1}{U_{1_\infty}}\right)^5 \left(\frac{T_e}{T_0}\right)^{1.56} \left(\frac{T_e}{T_w}\right)^{0.24} d\left(\frac{s'}{c'}\right) \quad , \tag{4}$$

where $R_{c'} = \dfrac{U_\infty \cos \Lambda \, c'}{\nu_\infty}$, and $\mu \propto T^n$ along the boundary layer, whilst across the layer $\mu \propto T$.

From the assumed Pohlhausen profiles, relationships between parameters in the related incompressible flow can be found. For example,

$$\lambda_i = -\left(\frac{\theta_{x_i}}{\nu_i}\right)^2 \left(\frac{dU_1}{ds'}\right)_i = \Lambda_i \left(\frac{37}{315} - \frac{\Lambda_i}{945} - \frac{\Lambda_i^2}{9072}\right)^2 \quad , \tag{5}$$

and by analytical inversion,

$$\Lambda_i = -\left(\frac{\delta_{x_i}}{\nu_i}\right)^2 \left(\frac{dU_1}{ds'}\right)_i = \left(1 - \sqrt{1 - \frac{675}{64}\lambda_i}\right)(13.74 - 17.04\lambda_i) \quad ,$$

$$\text{if } 0 \leqslant \lambda_i \leqslant 0.09 \quad , \tag{6a}$$

---

* This choice in fact leads to the answer being independent of the reference state in the Rott transformation.

and

$$\Lambda_i = 70\lambda_i \quad , \qquad \text{if } -1.4 \leqslant \lambda_i < 0 \quad . \tag{6b}$$

Hence the chordwise velocity profile is found:

$$\frac{u'}{U_1} = 2\eta - 2\eta^3 + \eta^4 + \Lambda_i \eta(1-\eta)^3/6 \quad , \tag{7}$$

where

$$\eta = z/\delta_x \quad . \tag{8}$$

Equation (4) is integrated numerically assuming a quadratic variation of the integrand with respect to s'/c' and using three neighbouring values at a time.

(c) The spanwise solution

In incompressible flow the momentum integral equation is, following Nath's notation broadly:

$$\frac{d}{ds'}(S\theta_x U_1)_i = \frac{0.225\nu_i}{\theta_{x_i} Q_i} \quad , \tag{9}$$

where

$$S = \frac{\theta_{xy}}{\theta_x} = \frac{\theta_{xy}/\delta_x}{\theta_x/\delta_x} \quad , \tag{10}$$

and

$$Q = \frac{\theta_y}{\theta_x} = \frac{\theta_y/\delta_y}{\theta_x/\delta_x}\frac{\delta_y}{\delta_x} \quad . \tag{11}$$

The Rott transformation does not affect the spanwise velocities (v) so that $Q = Q_i$, $S = S_i$, but we find that,

$$\theta_y = \theta_{y_i}\left(\frac{T_e}{T_{ref}}\right)^{\frac{5+r}{2}} \quad , \tag{12}$$

$$\theta_{xy} = \theta_{xy_i}\left(\frac{T_e}{T_{ref}}\right)^{\frac{5+r}{2}} \quad , \tag{13}$$

and

$$H_{x_i} = (1 + H_x)\frac{T_e}{T_w} - 1 \quad . \tag{14}$$

Hence, the compressible form of equation (9) becomes,

$$\frac{d}{d\frac{s'}{c'}}\left[S\frac{\theta_x}{c'}\frac{U_l'}{U_{l_\infty}}\left(\frac{T_e}{T_0}\right)^{2.5}\right] = \frac{0.225}{\frac{\theta_x}{c'}QR_{c'}}\left(\frac{T_\infty}{T_0}\right)^{1.74}\left(\frac{T_e}{T_w}\right)^{0.24}\left(\frac{T_e}{T_0}\right)^{0.76} \quad . \tag{15}$$

Equation (15) can be integrated for S (or Q) as dependent variables, once θ_x is known, provided that some assumption about the spanwise velocity profile *shape* is made (thereby providing another relation between S, Q and the known chordwise profiles). This spanwise profile, as mentioned earlier, is assumed to be given by the flat plate member of the Pohlhousen family, namely,

$$\frac{v'}{V_l} = \frac{v'}{U_\infty \sin\Lambda} = 2k\eta - 2k^3\eta^3 + k^4\eta^4 \quad , \tag{16}$$

where the length scale,

$$k = \frac{\delta_x}{\delta_y} \quad , \tag{17}$$

is to be calculated.

'Mixed' profile integrals, such as θ_{xy}, involving both velocity components can be evaluated as functions of Λ_i and k. This leads to the required relationships for $S(\Lambda_i,k)$ and $Q(\Lambda_i,k)$:-

$$S = S_i = \frac{\theta_{xy_i}}{\theta_{x_i}} = \frac{\left(\frac{3}{10} + \frac{\Lambda_i}{120}\right) - k\left(\frac{13}{15} + \frac{\Lambda_i}{180}\right) + k^3\left(\frac{67}{140} + \frac{\Lambda_i}{840}\right) - k^4\left(\frac{7}{36} + \frac{\Lambda_i}{3024}\right)}{\frac{37}{315} - \frac{\Lambda_i}{945} - \frac{\Lambda_i^2}{9072}} \quad , \tag{18}$$

and

$$Q = Q_i = \frac{\theta_{y_i}}{\theta_{x_i}} = \frac{37}{315}\left[k\left(\frac{37}{315} - \frac{\Lambda_i}{945} - \frac{\Lambda_i^2}{9072}\right)\right]^{-1} \quad . \tag{19}$$

Now, as $\Lambda_i(s')$ is known from the chordwise solution, we can write equation (15) as,

$$\frac{d[AS(k)]}{ds'} = \frac{0.225B}{R_{c'}} [Q(k)]^{-1} \quad , \tag{20}$$

where $A(s')$ and $B(s')$ are known functions.

Integrating, by means of the Trapezium Rule, gives,

$$[S]_{s'+\Delta s'} = \frac{1}{[A]_{s'+\Delta s'}} \left\langle - [AS]_{s'} + \frac{0.225}{R_{c'}} \frac{\Delta s'}{2} \{[BQ]_{s'+\Delta s'} + [BQ]_{s'}\} \right\rangle \quad . \tag{21}$$

Equations (18) and (21) both give values of S at the end of the step (i.e. at $s' + \Delta s'$) once k and hence Q are guessed. Three values disposed about the upstream value (at s') are used and quadratic interpolation is used to find the value of k that makes both values of S equal.

$\Delta s' = 0.01c'$ is used in the present program except, as described earlier in section 2.1.2(a), near to a sharp leading-edge velocity peak.

(d) Laminar separation

When $\lambda_i \to 0.09$ and hence $c_{f_{x'}} \to 0$, from the chordwise solution, separation is reached. The calculation is continued with $\lambda_i = 0.09$, $c_{f_{x'}} = 0$, across the entire chord.

(e) Leading-edge attachment line conditions

The values of $Q = 1.44$, $\lambda_i = -0.075$ are assumed, compatible with the results of Rott and Crabtree[17] for the yawed circular cylinder.

2.2.2 Transition assumptions

Cooke[6] showed that the spanwise and the chordwise components of momentum defect in the boundary layer must remain unchanged across the transition front on an infinite yawed wing. As, in the present method, we change from a chordwise/spanwise solution in the laminar layer to a solution in terms of local streamwise and cross-flow quantities in the turbulent flow, the quantities in these different coordinate systems must be related. Using a notation compatible with Nath we have,

$$\rho_e U_e^2 \theta'_{11} \equiv \rho_e U_1^2 \theta_x \quad ,$$

$$= \rho_e U_e^2 \left[\theta_{11} \cos^2 \phi - (\theta_{12} + \theta_{21}) \sin \phi \cos \phi + \theta_{22} \sin^2 \phi \right] \quad , \quad (22)$$

and

$$\rho_e U_e^2 \theta'_{21} \equiv \rho_e V_1 U_1 \theta_{xy} \quad ,$$

$$= \rho_e U_e^2 \left[(\theta_{11} - \theta_{22}) \sin \phi \cos \phi + \theta_{21} \cos^2 \phi - \theta_{12} \sin^2 \phi \right] \quad . \quad (23)$$

An iterative solution for the initial turbulent conditions is achieved by assuming, in addition to the above, that the streamwise velocity profile at the start of the turbulent flow has a local equilibrium form given by $G(\pi)$ - compatible with the assumptions in two-dimensions used previously by Nash *et al*[18]. The numerical calculation commences with a flat plate value of $G = 6.5$, and the approximation that $\theta_{11} = \theta_x$ in equation (22).

The velocity profile and skin-friction assumptions of Nash[7] are then used to find an improved estimate for G, as follows:

$$c_f = f(F_r, F_c, R_{\theta_{11}}, G) \quad ,$$

$$H = 0.228 M_e^2 + \frac{\left(1 + 0.135 M_e^2\right)}{\left(1 - G\sqrt{c_f/2}\right)} \quad , \quad (24)$$

from the use, by Nash, of an improved correlation of experimental data[19] instead of the usual assumptions, given later as equation (26).

Thus we have,

$$\pi = \frac{H}{\theta_{11}} \frac{dp}{ds'} \frac{\cos \phi}{\tau_{w_1} \cos \beta} \quad , \quad (25)$$

using local streamwise components and hence,

$$G = 6.1\sqrt{\pi + 1.81} - 1.7 \quad , \quad (26)$$

from Ref.18.

Equation (22) × tan ϕ + equation (23) then yields an equation from which a better approximation to β_T can be obtained, namely:

$$\tan \beta_T = \frac{\theta_{11}(1 + \tan^2 \phi) - \theta_x - \theta_{xy} \tan^2 \phi}{\bar{\delta}(1 + \tan^2 \phi) \tan \phi \, w_4(n)} \quad , \tag{27}$$

where $w_4(n) = \theta_{12}/\bar{\delta} \tan \beta$ as described later, in section 2.3.1(d).

The turbulent profile properties are then evaluated and an improved estimate of θ_{11} is obtained using equation (22) in the form

$$\theta_{11} = \theta_x + \left[(\theta_{12} + \theta_{21}) \tan \phi - \theta_{22} \tan^2 \phi\right] \quad . \tag{28}$$

This method of solution was not convergent unless an under-relaxation factor of 0.5 was introduced.

The present physical assumptions and the numerical treatment are capable of improvement although, as mentioned in Part III[1] of this series of papers, qualitatively correct behaviour of the surface cross-flow angle is achieved in adverse pressure gradient conditions.

2.3 The turbulent boundary layer

2.3.1 The entrainment integral method in compressible flow

(a) The basic equations

The present method uses three simultaneous first order differential equations describing the development of streamwise momentum thickness (θ_{11}), cross-flow thickness (for example θ_{12}) and, using the entrainment equation, the development of Δ. These equations are derived, for compressible flow on an infinite yawed wing, by Smith[10], and are summarized here and on Figs.6, 7 and 8 as:

$$\frac{d\theta_{11}}{ds} = \frac{c_{f_1}}{2} + \theta_{11}\left[K_1 - \left(H + 2 - M_e^2\right)\frac{1}{U_e}\frac{dU_e}{ds}\right] - K_1\theta_{22} - \theta_{12}\left[M_e^2 \tan \phi \frac{1}{U_e}\frac{dU_e}{ds}\right] + \frac{d\theta_{12}}{ds} \tan \phi \, . \tag{29}$$

$$\frac{d\theta_{12}}{ds} = \frac{c_{f_1} \tan \beta}{2} + \theta_{12}\left[2K_1 + \left(M_e^2 - 2\right)\frac{1}{U_e}\frac{dU_e}{ds}\right] + \theta_{22}\left(1 - M_e^2\right)\frac{\tan \phi}{U_e}\frac{dU_e}{ds}$$

$$+ \theta_{11}(1 + H)\frac{\tan \phi}{U_e}\frac{dU_e}{ds} + \tan \phi \frac{d\theta_{22}}{ds} \quad . \qquad (30)$$

$$\frac{d\Delta}{ds} = F(H_1) - \Delta\left[\left(1 - M_e^2\right)\frac{1}{U_e}\frac{dU_e}{ds} - K_1\right] + \delta_2^*\left[\frac{M_e^2}{U_e}\frac{dU_e}{ds}\tan \phi\right] - \frac{d\delta_2^*}{ds}\tan \phi \quad . (31)$$

For their solution, assumptions for entrainment rate (F), streamwise skin-friction (c_{f_1}) and both the streamwise and the cross-flow velocity profiles are needed. These are broadly similar to the assumptions used by Cumpsty and Head[9] with the addition of compressibility effects along the lines, proposed for two-dimensional flow, by Green[11] and by Nash[13].

(b) Streamwise velocity profiles

In the local external streamwise direction the shape factors are related as follows:-

For $M_e \leqslant 0.3$, the original relationship for incompressible flow due to Head[15] is approximated analytically as suggested by Thompson[20]. Separation is assumed to occur when $H_1 = 3.5$; we therefore take, in the range $3.5 \leqslant H_1 \leqslant 5.3$,

$$\bar{H} = \exp(-0.1511 - 0.777 \log_e (H_1 - 3.3)) + 1.1 \quad , \qquad (32)$$

and for $H_1 > 5.3$,

$$\bar{H} = \exp(0.143057 - 0.326375 \log_e (H_1 - 3.3)) + 0.6798 \quad . \qquad (33)$$

If $M_e > 0.3$, the relationship used is that, proposed for compressible flow, by Green[12]. Separation is now assumed to occur at $H_1 = 3.74$; we therefore take, for $H_1 \geqslant 3.74$,

$$\bar{H} = 1 + 1.12\left(H_1 - 2 - \sqrt{(H_1 - 2)^2 - 3}\right)^{0.915} \quad , \qquad (34)$$

where $\bar{H}$ is taken as the best analogue in compressible flow to H in incompressible flow, and assuming a recovery factor of $r = 0.89$, these are related by

$$H = \frac{T_w}{T_e}\bar{H} + \frac{T_r}{T_e} - 1 \quad , \tag{35}$$

$$= \left(1 + 0.2M_e^2\right)\bar{H} + 0.178M_e^2 \quad . \tag{36}$$

Green assumes that the total temperature is constant across the boundary layer and hence that $T_w = T_{0e}$.

(c) Skin-friction relationships

A simple relationship is used as proposed by Green[12], based on a generalisation of the form given by Spalding and Chi[21] for zero pressure gradient, but in the present work the analytical forms for the Spalding and Chi functions F_r, F_c are those given originally by Nash *et al*[7].

Summarizing these expressions, we have:

$$c_{f_1} = c_{f_0}\left(\frac{0.9}{(\bar{H}/\bar{H}_0 - 0.4)} - 0.5\right) \quad , \tag{37}$$

$$\bar{H}_0 = \left(1 - 6.8\sqrt{c_{f_0}/2}\right)^{-1} \quad , \tag{38}$$

$$c_{f_0} = \left[\frac{0.012}{\left(\log_{10}\left(F_r R_{\theta_{11}}\right) - 0.64\right)} - 0.00094\right]\frac{1}{F_c} \quad , \tag{39}$$

where

$$F_c = \left(1 + 0.066 \times M_e^2 - 0.008 \times M_e^3\right)^2 \quad , \tag{40}$$

and

$$F_r = 1 - 0.134 \times M_e^2 + 0.027 \times M_e^3 \quad . \tag{41}$$

The subscript '0', used by Green, refers to nominal flat plate zero pressure gradient conditions and his expressions can be shown to agree well with the full two-parameter skin-friction law proposed for incompressible flow by Thompson[22] as well as being supported by the skin-friction data that were

(d) Cross-flow assumptions

Here the simple treatment first used by Cumpsty and Head[9] and by Smith[10] is retained. That is, the cross-flow velocities within the layer are related to the surface angle β using the simple expression, due to Mager[23]

$$\frac{v}{u_s} = (1 - \eta)^2 \frac{u}{U_e} \tan \beta \quad , \tag{42}$$

with power law streamwise velocity profiles,

$$\frac{u}{U_e} = \eta^n \quad , \tag{43}$$

where

$$n = \frac{\bar{H} - 1}{2} \quad , \tag{44}$$

employed to achieve simple analytical expressions, for the cross-flow integral parameters and their derivatives with respect to surface distance (s), in terms of the basic dependent variables of the problem. Compressibility effects are introduced, as suggested by Green[11], by introducing the transformation,

$$d\eta = \frac{\rho}{\rho_e} \frac{dz}{\bar{\delta}} \quad , \tag{45}$$

where

$$\bar{\delta} = \int_0^{\delta} \frac{\rho}{\rho_e} dz \quad . \tag{46}$$

Hence, for example, we have,

$$n = \frac{\bar{H} - 1}{2} = \frac{1}{H_1 - 2} \quad , \tag{47}$$

where $H_1 = \Delta/\theta_{11}$,

$$\Delta = \bar{\delta}\left(\frac{1}{n + 1}\right) \quad , \tag{48}$$

$$\theta_{11} = \bar{\delta}\left[\frac{n}{(2n + 1)(n + 1)}\right] \quad , \tag{49}$$

$$\left.\begin{aligned} \theta_{12} &= \bar{\delta}\,\tan\beta\, w_4(n) \quad , \\ \theta_{22} &= \bar{\delta}\,\tan^2\beta\, w_1(n) \quad , \\ \theta_{21} &= \bar{\delta}\,\tan\beta\, w_3(n) \quad , \\ \delta_2^* &= \bar{\delta}\,\tan\beta\, w_2(n) \quad . \end{aligned}\right\} \tag{50}$$

The functions $w_i(n)$ are defined as follows:

$$\left.\begin{aligned} w_1(n) &= -\frac{1}{(2n+1)} + \frac{4}{(2n+2)} - \frac{6}{(2n+3)} + \frac{4}{(2n+4)} - \frac{1}{(2n+5)} \quad , \\ w_2(n) &= -\frac{2}{(2n+2)} + \frac{4}{(2n+4)} - \frac{2}{(2n+6)} \quad , \\ w_3(n) &= -\frac{1}{(2n+1)} + \frac{2}{(2n+2)} - \frac{1}{(2n+3)} \quad , \\ w_4(n) &= -\frac{1}{(2n+1)} + \frac{4}{(2n+2)} - \frac{1}{(2n+3)} - \frac{4}{(2n+4)} + \frac{2}{(2n+6)} \quad . \end{aligned}\right\} \tag{51}$$

(e) The entrainment function

The simple analytical approximation, proposed originally by Thompson[20] to fit Head's curve for incompressible flow, has been assumed to hold for all conditions of compressible flow. That is,

$$F = 0.0299(H_1 - 3)^{-0.617} \quad . \tag{52}$$

2.3.2 The numerical solution

After rewriting the cross-flow equation (30) as a differential equation for $\tan\beta$, Cumpsty and Head[9] solved the equations (29), (30) and (31) numerically by means of a global iteration technique. They preferred this method, because of its physical clarity, to a step-by-step method. The latter method also appeared to them to be less stable near separation. The present authors began therefore by programming this global iteration method. However, it was found to converge very slowly near to separation, as Fig.3 shows, and was eventually discarded because, in the region of favourable pressure gradient just downstream of the swept attachment line, it becomes oscillatory and divergent even with strong artificial damping incorporated (see Figs.4 and 5).

This global iteration method solves the complete boundary-layer development using the streamwise momentum equation (29) and entrainment equation (31) with a fixed cross-flow development $\beta(s)$ obtained from the previous separate solution of the cross-flow equation. The solution of the latter is then updated using, as fixed data, the developments of $\theta_{11}(s)$, $\Delta(s)$ from the solution of the other two equations. The damping used by the present authors was applied as follows:

$$\left[\frac{df}{ds}\right] = \left[\frac{df}{ds}\right]_j P + \left[\frac{df}{ds}\right]_{j-1} (1 - P) \quad , \tag{53}$$

$$f_j(s) = \Delta s \left[\frac{df}{ds}\right] + f_j(s - \Delta s) \quad , \tag{54}$$

where f represents any of the dependent variables concerned and $[df/ds]$ stands for the derivative at the middle of the current step Δs, and j is the global iteration count. The initial (axisymmetric) approximation, corresponding to the curve for $j = 0$ in Figs.4 and 5, assumes that $\beta = 0$ everywhere.

The equations were therefore rewritten, using the profile relationships of 2.3.1(d), explicitly in terms of the three variables θ_{11}/c', Δ/c' and $\tan\beta$. These equations were solved by matrix inversion, iterating until the mid-step derivatives gave successive calculated values that differed by less than 1%. No convergence problems were encountered over a range of step lengths (Δs) between 1 and 20 local boundary-layer thicknesses ($\bar{\delta}$). This is shown, in Figs.20 and 21, for the practical test case considered in detail later in section 3. The calculation time for Cumpsty and Head's test case at $\Lambda = 35^o$ was reduced from 22 minutes on KDF 9 to less than 1 minute (including considerable print-out).

The reasons for the difficulties encountered by the global iteration procedure are readily explained by reference to Figs.6a to 8b inclusive. In these figures the terms in each of the basic equations (29), (30) and (31) are plotted out for the complete boundary-layer development on the highly swept wing of Cumpsty and Head[24,25]. In each case the figures are divided into,

(a) adverse pressure gradient, and

(b) (leading edge) favourable pressure gradient regions.

Figs.6a, 6b show that the 'correction term' (i.e. all the quantities involving the cross-flow β) used in the global iteration method for solving the streamwise momentum integral equation (29) includes a derivative of the cross-flow properties. This quantity, namely $\tan \phi \ (d\theta_{12}/ds)$, is no longer small, compared with the derivative $(d\theta_{11}/ds)$ being calculated, once separation is approached (see Fig.6b) and becomes much larger than $d\theta_{11}/ds$ close to the attachment line where (see Fig.6a) the rate of growth of θ_{11} along an external streamline is very small. Similar comments are appropriate to the corrections applied to the other equations and account for the difficulties with the global iteration method.

The pressure distribution used in the foregoing calculations is labelled 'B' in Fig.9 and the angle of sweep $\Lambda = 62.5^{o}$ has been assumed. Surface and external streamline shapes for both interpretations 'A' and 'B' of this experimental arrangement are shown in Fig.10.

Further discussions of this experiment and the various theoretical predictions that have been made are given in Refs.26 and 27, and need not be repeated here, as we are at present concerned primarily with the relative orders of the terms in the equations once having found the best interpretation of the pressure data (and isobar sweep) to give reasonable agreement with the observed rear separation.

Interest in separating out the various terms of the equations was also occasioned by the hope that some terms would prove to be very small and hence that a worthwhile simplification could be introduced into the equations. However, this turns out to be a dangerous idea as the only small terms are those (as Figs.6a to 8b show) where local Mach number enters as M_e^2 and hence are small for a lowspeed flow but would not be expected to remain small at transonic speeds.

2.3.3 Turbulent attachment line flow

(a) Calculation of compressible attachment line flow

The introduction of compressibility means that the turbulent attachment line properties are now functions of C* and the Mach number, $M_{a.l.}$ of the flow along the attachment line. Following the first method of prediction explained in Cumpsty and Head's paper[8] the cross-flow equation (30) is differentiated with respect to surface distance normal to the attachment line and solved simultaneously with the streamwise momentum equation and entrainment

equations to yield solutions for the three principal dependent variables $R_{\theta_{11}}$, $\theta_{11}(\partial\beta/\partial s')$, and n. The equations and the assumptions for entrainment, skin-friction and for velocity profile shape in compressible flow have already been given for the general infinite yawed wing case in section 2.3.1. The attachment line assumptions are entirely consistent with the general method but the associated set of equations was solved separately once for all in the range,

$$0 \leqslant M_{a.l.} \leqslant 2 \quad , \tag{56}$$

$$7 \times 10^4 \leqslant C^* \leqslant 10^7 \quad , \tag{57}$$

for which fully turbulent flow was assumed. On the attachment line equations (29), (30) and (31) become,

$$\frac{d\delta_2^*}{ds'} = F(H_1) - \Delta \frac{K}{\tan \Lambda} \quad , \tag{58}$$

$$-\frac{d\theta_{12}}{ds'} = \frac{c_{f_1}}{2} - \theta_{11} \frac{K}{\tan \Lambda} \quad , \tag{59}$$

and

$$\frac{d\theta_{22}}{ds'} = 0 \quad , \tag{60}$$

where

$$K = \frac{R_{\theta_{11}}}{C^*} \frac{\tan \Lambda}{\theta_{11}} \quad . \tag{61}$$

These are formally identical to the equations of Ref.8 for incompressible flow. However, c_{f_1}, F and the velocity profile relationships will introduce implicitly a dependence on $M_{a.l.}$. Equation (60) is of no use as it stands and it is necessary to differentiate the cross-flow momentum equation with respect to s', giving,

$$\frac{d\theta_{21}}{ds'} \frac{3K}{\tan \Lambda} - \frac{d^2\theta_{22}}{d(s')^2} - \frac{K^2}{\tan^2 \Lambda} \left\{ \theta_{11} + \delta_1^* \right\} = \frac{c_{f_1}}{2} \frac{d\beta}{ds'} \quad . \tag{62}$$

Introducing the velocity profile assumptions of section 2.3.1(b) we find that,

$$\frac{d^2\theta_{22}}{d(s')^2} = 2w_1(n)\bar{\delta}\left(\frac{d\beta}{ds'}\right)^2 \quad , \tag{63}$$

on the attachment line and the equations (58), (59) and (62) become three simultaneous non-linear algebraic equations for the dependent variables $R_{\theta_{11}}$, n and Z, where $Z = \theta_{11}\,(d\beta/ds')$.

That is,

$$F(H_1) = H_1 \frac{R_{\theta_{11}}}{C^*} = w_2(n)\,\frac{\bar{\delta}}{\theta_{11}}\,Z \quad , \tag{64}$$

$$\frac{c_{f_1}}{2} - \frac{R_{\theta_{11}}}{C^*} = -\,w_4(n)\,\frac{\bar{\delta}}{\theta_{11}}\,Z \quad , \tag{65}$$

and

$$2w_1(n)\left(\frac{\bar{\delta}}{\theta_{11}}\right)^2 Z^2 + Z\left\{\frac{c_{f_1}}{2} - 3\left(\frac{R_{\theta_{11}}}{C^*}\right)\frac{\bar{\delta}}{\theta_n}\,w_3(n)\right\} + \left(\frac{R_{\theta_{11}}}{C^*}\right)^2 \frac{\bar{\delta}}{\theta_{11}}\left\{1 + H\right\} = 0 \quad . \tag{66}$$

Solution is effected by solving the quadratic equation (66) for Z, assuming values of n and of $R_{\theta_{11}}$. The negative root is taken as the pressure gradient normal to the external streamlines must give rise to an initially negative sign for $d\beta/ds'$. Substitution of Z into the remaining equations (64) and (65) then yields two simultaneous equations for $R_{\theta_{11}}$ and n. A double iteration process converges rapidly to give the results which have been analytically approximated by the expressions given in the Appendix, and are used in the design program in that form. This procedure results in considerable economy of computing time compared with a solution of the full equations every time a boundary-layer calculation is needed. Figs.11, 12 and 13 summarise the present results for $M_{a.l.} = 0$, 1 and 2 in the range $7 \times 10^4 \leqslant C^* \leqslant 5 \times 10^5$.

The shape factor $\bar{H}$ is presented in Fig.13 instead of n (as used in the Appendix) as comparison with Cumpsty and Head's measurements can be made in a more familiar way. The general level of agreement with experiment for their incompressible flow is, as Ref.8 showed earlier, not especially good even for momentum thickness (see Fig.11). However, it must be remembered that even

the latest differential methods of turbulent boundary-layer prediction, such as that of Bradshaw[14], give only a modest level of agreement with these measurements. Very recently, Crabbe[28] has shown how turbulent structure and hence entrainment rate depends on lateral stretching so that it may now be possible to improve the integral method although the greatest improvement would be possible through the use of better skin-friction and velocity profile assumptions at these low Reynolds numbers.

(b) Initial values, for the turbulent calculation, just downstream of the attachment line

Each dependent variable can be represented by a Taylor series in terms of surface distance normal to the attachment line. That is, for example,

$$\theta_{11}\left(\frac{s_i'}{c'}\right) = (\theta_{11})_{a.l.} + \frac{s_i'}{c'}\left[\frac{d\theta_{11}}{d\,\frac{s'}{c'}}\right]_{a.l.} + \ldots \qquad (67)$$

with Δ/c' or $\bar{H}$ represented similarly; whilst for the cross-flow angle (β) we have,

$$\beta\left(\frac{s_i'}{c'}\right) = 0 + \frac{s_i'}{c'}\frac{\left[\theta_{11}\,\frac{d\beta}{d\,\frac{s'}{c'}}\right]_{a.l.}}{\left[\frac{\theta_{11}}{c'}\right]_{a.l.}} + \ldots \quad . \qquad (68)$$

For simplicity, and in view of the modest level of accuracy of the attachment line predictions themselves, the first non-zero term in each expansion has been used alone to represent the entire series. Typical results, for a range of starting distances (s_i'/c'), are shown in Figs.14 to 16, for the case of a yawed circular cylinder of radius R in incompressible flow. In this simple case $c' = 2R$. Convergent behaviour is shown for

$$0.0005 \leqslant \frac{s_i'}{c'} \leqslant 0.05 \text{ radians} \quad . \qquad (69)$$

Fig.17 confirms this convergence as far as predictions for $R_{\theta_{11}}$ up to rear separation are concerned. A value of 0.001 has been used in all subsequent

routine calculations (as in Ref.1) for design purposes and this ensures adequate accuracy as in practice the effective radius (σ') of the cylinders is between 1% and 5% of c'. Hence we normally take $s_i'/c' = 0.00001$ to 0.00005 as the starting values.

2.3.4 Behaviour near to separation

This has been discussed rigorously by Myring[29] for the present integral equations and cross-flow profile assumptions. He found that the equations formed a hyperbolic set whose outer characteristic lags on the surface streamline and hence becomes parallel to the generators of an infinite yawed wing downstream of the true separation line.

The present authors have attempted no such detailed numerical analysis although they realised that these properties were likely from the earlier analyses of Mager[23] and Raetz[30]. No problems in using the present step-by-step procedure have been encountered and indeed calculations have been taken past the predicted line of rear separation with the idea of giving a rough estimate of the initial rapid increase in profile drag and in displacement thickness when small regions of separated flow could be present (see Part III [1] for typical results).

Separation occurs (strictly) when the predicted surface streamlines become parallel to the generators of the infinite wing; that is, when,

$$\beta + \phi = 90^{\circ} \quad ,$$

or equivalently,

$$c_{f_{x'}} = 0 \quad .$$

The turbulent boundary-layer predictions are continued beyond separation if this occurs for $x'/c' = 0.9$, by setting

$$\tan \beta = \frac{0.999}{\tan \phi} \quad , \tag{70}$$

if the calculated value of $\tan \beta$ is greater than that quantity.

c_{f_1} is limited to not less than 10^{-6}, and H_1, $\bar{H}$ and hence F are constrained at their separation values.

2.3.5 Displacement thickness

The full expression for displacement effect as given originally by Lighthill[31] is used, which as Cooke[32] showed becomes for infinite yawed wings:

$$\delta^* = \delta_1^* - \delta_2^* \tan \phi \quad . \tag{71}$$

2.3.6 Possible laminar reversion

The inner region pressure gradient parameter ($\Delta_{\ell s}$) evaluated on the basis of the component of pressure gradient taken in the direction of the local surface shear vector $\underline{\tau_w}$ is,

$$\Delta_{\ell s} = \frac{\nu_w}{U_\tau^3} \frac{1}{\rho_w} \frac{dp}{ds'} \cos(\phi + \beta) \quad . \tag{72}$$

It is assumed, following Patel's[33] work in two-dimensions, that the simple fully turbulent inner region relationships will break down if the magnitude of this quantity exceeds about 0.01. In favourable pressure gradients this is an indication of onset of reversion to laminar flow and, as described in Ref.2, can occur even in flight conditions just downstream of typical swept attachment line flows which are themselves likely to be fully turbulent especially with contamination from the fuselage boundary layer.

2.4 The turbulent wake and prediction of profile drag

The coefficient of profile drag (as in the results of Ref.1) is found by using the expression derived by Cooke[6]:

$$C_D = 2\left(\theta'_{11_\infty} \cos^3 \Lambda + \theta_{21_\infty} \sin \Lambda\right) \quad , \tag{73}$$

where the independence principle is invoked to allow separate solution for the chordwise momentum integral equation (relating $\theta'_{11_{t.e.}}$ to θ'_{11_∞}) and the spanwise momentum integral equation (relating $\theta'_{21_{t.e.}}$ to θ'_{21_∞}).

The spanwise solution is the same as used by Cooke, namely,

$$\theta'_{21_\infty} = \left(\frac{U_e}{U_\infty}\right)^2_{t.e.} \times \theta'_{21_{t.e.}} \times \left(\frac{T_e}{T_\infty}\right)^{2.5}_{t.e.} \quad , \tag{74}$$

whilst the chordwise solution is taken to be compatible with the expression commonly used in the method for predicting profile drag in two-dimensions. This is an empirical modification of the compressible Squire/Young formula proposed by Nash and reported in Ref.34. That is

$$\theta'_{11_\infty} = \theta'_{11_{t.e.}} \times \left(\frac{T_e}{T_\infty}\right)^3_{t.e.} \times \left[\frac{U_e \cos\phi}{U_\infty \cos\Lambda}\right]^\chi_{t.e.} \quad , \tag{75}$$

where $$\chi = 0.28571\left(1 + H'_{t.e.}\right)\frac{T_\infty}{T_0} + 2.4286 \quad , \tag{76}$$

$$H' = \frac{\delta_1^{*'}}{\theta'_{11}} \quad , \quad \text{and} \quad \delta_1^{*'} = \delta_1^* - \tan\phi\,\delta_2^* \quad . \tag{77}$$

The dashed quantities are evaluated for chordwise velocities and are related (as shown by Cooke) to the usual streamwise and cross-flow integrals at the trailing edge by the following expressions (which are rewritten versions of equations used already in section 2.3.1)

$$\theta'_{11} = \theta_{11} - \tan\phi\,(\theta_{21} + \theta_{12}) + \tan^2\phi\,\theta_{22} \quad , \tag{78}$$

and

$$\theta'_{21} = (\theta_{11} - \theta_{22})\sin\phi\cos\phi + \theta_{21}\cos^2\phi - \theta_{12}\sin^2\phi \quad . \tag{79}$$

3 RESULTS OF COMPUTATIONS FOR PRACTICAL TEST CASES

The boundary-layer calculations were made using measured lower surface pressures on the RAE(NPL) 9510 section at $M_\infty \cos\Lambda = 0.76$. This section is heavily rear-loaded as the distribution of external velocity shown here in Fig.18, reveals. The weak shock present at the position of maximum velocity has been slightly smoothed to avoid difficulties with numerical differentiation of the test data. The original measurements[35] were made on a two-dimensional section in the 36in × 14in transonic wind tunnel at RAE Teddington at a chord Reynolds number of about 3.6×10^6. The present calculations were made, however, for assumed flight conditions of $\Lambda = 30^\circ$, $R_c = 40 \times 10^6$ and hence for $M_\infty = 0.878$, which are typical of an advanced modern transonic transport aircraft. The surface streamlines and the external potential-flow streamlines, predicted for this condition, are shown in Fig.19.

The flow is fully turbulent across the entire chord and the developments of $R_{\theta_{11}}$ and of β are as shown respectively in Figs.20 and 21. As mentioned

earlier (in section 2.3.2) the numerical results agree over a 20:1 range of step lengths.

The severity and the usefulness of this test case is especially clearly shown in Fig.21 where the rapid variations in cross-flow angle β, including the effects of *two* changes in sign of the transverse pressure gradient, are apparent. The sensitivity of predictions to cross-flow profile assumptions in this case should be conclusive proof that improvements to these assumptions were required or not.

Fig.22 shows the effect of step length upon the relative times (proportional to the number of iterations of the stepwise solution of the differential equations) taken for the basic turbulent calculation. In the parametric study of Ref.1, the step lengths $\Delta s = 10\bar{\delta}$ or $0.025c'$ were used. No practical advantages result from increasing the step size further.

The lower curves show that a large proportion of the total calculation time is spent on that part of the boundary-layer development close to the leading edge. About 40% of the calculation time is spent in reaching $0.01c'$ and about 55% in reaching $0.1c'$.

Finally, in Figs.23 and 24, some results are shown, appropriate to the wing study of Ref.1, in which a rather less advanced aerofoil was used (RAE (NPL) 3111). Calculation time (see Fig.23) increases roughly in proportion to the total path length (s) of the turbulent boundary layer along an external streamline, for a given leading-edge condition and a given value of streamwise chord Reynolds number (R_c). The corresponding dependency upon angle of sweep (Λ) is shown also in Fig.23. The sudden fall in computing time associated with establishing turbulent attachment line flow is explained by Fig.24 where the turbulent boundary-layer thickness at or near to the start of the calculation (that is at $x'/c' = 0.0155$) is seen to increase suddenly once the flow becomes fully turbulent at the attachment line. This, of course, is a result of the abrupt transition assumed to occur when $C^* = 10^5$, whereas, in practice, a gradual change of boundary-layer conditions would occur at the swept attachment line and hence at the beginning of the calculated region as Λ (and hence C^*) increased.

The above results should give the user some idea of the performance of the complete program in a form that is likely to be independent of the particular computer available to him. The typical time for a boundary-layer calculation for one wing surface on the KDF 9 computer is 30 seconds, including allowance for extensive print-out.

4 DISCUSSION

At various points in the above description of the method shortcomings have been recorded. In particular, the assumptions for transition are crude and as yet no reliable data exist from which they may be improved. Even the compressible laminary boundary-layer predictions have not been compared with the nominally exact numerical results that are now possible[36] although, except near to separation, this uncertainty is likely to lead to only very small errors.

The cross-flow assumptions in the turbulent boundary-layer calculation are incapable of accounting for inflections in the cross-flow velocity profile. The entrainment function is also (now) rather outdated by improvements in two-dimensional methods (for example, the lag-entrainment method[37]).

However, as pointed out by Thompson *et al.*[38] it is not necessary in design work to describe the details of the physical processes accurately. What *is* important is their influence on the overall answer for profile drag, displacement effect on lift curve slope, for example, and especially it is less important to predict quantitative levels than to predict exchange rates between these quantities.

Consequently, improving the turbulent boundary layer assumptions alone may or may not make sufficient difference to the predicted variations of $C_D(\Lambda,R_c)$, (say), to affect the designer. In this connection, it should be remembered that the best available differential method for three-dimensional flow[14] is about twenty times slower than current integral methods on a given computer, and also runs into problems at or near to the swept attachment line (see Ref.2). Also it is not, as yet, programmed for use in compressible three-dimensional conditions.

5 CONCLUSIONS

The description, given in section 2, of the complete calculation method suggests that:

(i) The use of the independence principle for compressible laminar flow is unlikely to lead to errors of practical importance for $\Lambda \leqslant 45^{\circ}$, unless separation is present.

(ii) Comparison should be made, for a fairly severe test case, however, between this simple method and the exact numerical procedures now available.

(iii) The present assumptions for transition are crude and require further examination.

(iv) The numerical method preferred by Cumpsty and Head for solving the integral form of the turbulent boundary-layer equations is not satisfactory near to separation or near to the swept leading-edge attachment line.

(v) Further investigation of the flow at and near to the swept attachment line is required.

The numerical test cases described in section 3 and the overall discussion, in section 4, show that:

(vi) In practical flight conditions the present numerical method is both satisfactorily fast, convergent and convenient to use.

(vii) Two strong reversals of transverse pressure gradient are possible and might be inadequately described by the present simple velocity profile assumptions.

(viii) However, the success of simple turbulent integral methods in two-dimensional flow, together with the presence of (probably) large errors due to lack of knowledge of transition and the difficulties encountered close to the swept attachment line by even the most sophisticated modern calculation methods reinforces the present author's opinion[38] that it is important to *use* the simple method for design purposes *now* in order to find out if difficulties occur to an extent that really would worry the designer in practice rather than reject a readily available and tested method on purely theoretical grounds.

Acknowledgments

The authors are indebted to Mr. B.J. Powell of Kingston Polytechnic for discussions over numerical methods, and to Dr. J.E. Green of RAE Bedford for making available, at an early stage, his assumptions for the effects of compressibility on the turbulent boundary layer.

Appendix

ANALYTICAL APPROXIMATIONS TO PREDICTIONS FOR COMPRESSIBLE TURBULENT ATTACHMENT LINE FLOW

$$R_{\theta_{11}} = \left\langle \left\{ \left[1 + 0.2(M_{a.l.})^2 \right] \Big/ \left(1 + 0.2M_\infty^2 \right) \right\}^{1.74} \Big/ \tan \Lambda / R_c \right\rangle \times \exp \left\{ -2.304 + 0.0231 M_{a.l.} + 0.0282(M_{a.l.})^2 + \left[0.581 - 0.016705 M_{a.l.} - 0.006615(M_{a.l.})^2 \right] \log_e C^* + \left[0.008575 + 0.001203 M_{a.l.} - 0.000178(M_{a.l.})^2 \right] \left(\log_e C^* \right)^2 \right\} . \quad \ldots \quad (A\text{-}1)$$

$$\theta_{11} \frac{d\beta}{ds^*} = - \left[0.038617 + 1.125 \times 10^{-4} M_{a.l.} + 1.25 \times 10^{-5} (M_{a.l.})^2 - 7.42 \times 10^{-3} \log_e z + 4.886 \times 10^{-4} (\log_e z)^2 - 1.0909 \times 10^{-5} (\log_e z)^3 \right] , \quad (A\text{-}2)$$

where

$$z = C^* \Big/ \left\{ 1 + 0.05 M_{a.l.} + 0.18(M_{a.l.})^2 \right\} . \quad (A\text{-}3)$$

$$n = \exp \left\{ 1.587 - 0.34(M_{a.l.}) + 0.21067(M_{a.l.})^2 - \left[0.3388 - 0.04429(M_{a.l.}) + 0.03161(M_{a.l.})^2 \right] \log_e C^* + \left[0.0076 - 0.0012803(M_{a.l.}) + 0.0009283(M_{a.l.})^2 \right] (\log_e C^*)^2 \right\} . \quad (A\text{-}4)$$

Note also that, from equation (47);

$$H_1 = \frac{1 + 2n}{n} , \quad (A\text{-}5)$$

and

$$\bar{H} = 1 + 1.12\left(H_1 - 2 - \sqrt{(H_1 - 2)^2 - 3}\right)^{0.915} . \qquad (34)$$

The percentage differences of the above formulae, (A-1) to (A-4), from the exact solutions of the equations are:

$M_{a.1.}$	$\theta_{11}\frac{d\beta}{ds^*}$	n	$R_{\theta_{11}}$
0.01	< 1% except near $C^* = 3 \times 10^6$	< 0.3%	< 0.9%
1.0	< 2% except near $C^* = 5 \times 10^5$	< 0.3%	< 0.3%
2.0	< 3% except near $C^* = 5 \times 10^5$	< 0.4%	< 0.9%

NOTATION

A, B functions appearing in the spanwise solution for the laminar boundary layer (see section 2.2.1(c))

c chord length in line of flight

c' chord length normal to generators (i.e. 'chordwise' chord = $c \cos \Lambda$)

C^* $= \dfrac{U_\infty^2 \sin^2 \Lambda}{\nu_{a.l.} \dfrac{d}{ds'}\left(\dfrac{U_l}{}\right)}$, attachment line parameter

C_D conventional profile drag coefficient

c_f $= \dfrac{\tau_w}{\frac{1}{2}\rho_e U_e^2}$, total skin-friction coefficient

c_{f_l} $= c_f \cos \beta$, component of skin-friction in direction of local external velocity $(\underline{U_e})$

$c_{f_{x'}}$ $= c_f \cos (\phi + \beta)$, chordwise component of c_f

C_p $= \dfrac{p - p_\infty}{\frac{1}{2}\rho_\infty U_\infty^2}$, conventional pressure coefficient

C_p^* $= C_p \sec^2 \Lambda$

c_p specific heat of fluid at constant pressure

F entrainment coefficient

F_c, F_r functions in the Spalding-Chi skin-friction law

Boundary layer shape factors based upon the components of velocity along and normal to the local external velocity $(\underline{U_e})$ direction:-

$$G = \sqrt{\frac{2}{c_{f_l}}} \frac{\int_0^\infty (U_e - u)^2 dz}{\int_0^\infty (U_e - u) dz}$$

H $= \delta^*/\theta_{ll}$

$\bar{H}$ $= \dfrac{1}{\theta_{ll}} \int_0^\infty \dfrac{\rho}{\rho_e}\left(1 - \dfrac{u}{U_e}\right) dz$, compressible analogue of H, as used by

NOTATION (continued)

H_1 $= (\delta - \delta^*)/\theta_{11} = \Delta/\theta_{11}$

shape factors appropriate to the chordwise and spanwise coordinates and velocity components:-

H_x $= \delta_x^*/\theta_x$, notation of Nath[4] - laminar

H' $= \delta_1^{*'}/\theta_{11}'$, notation of Cooke[6] - turbulent

K convergence rate of external streamlines $\left(= \sin\phi \frac{d\phi}{ds'}\right.$ for infinite yawed wings$\left.\right)$

k $= \delta_x/\delta_y$ in section 2.2.1(c)

M Mach number, e.g. M_e, M_∞

n exponent in temperature/viscosity law assumed in laminar flow, or exponent in power-law expressions for turbulent velocity profiles. (No ambiguity in the text.)

p local static pressure

p_0 local total pressure

P relaxation parameter used in section 2.3.2

Q, Q_i defined for laminar flow in section 2.2.1(c)

R_c $= \dfrac{U_\infty c}{\nu_\infty}$ streamwise (i.e. line of flight chord Reynolds number)

$R_{c'}$ $= \dfrac{U_\infty \cos\Lambda c'}{\nu_\infty} = R_c \cos^2\Lambda$

$R_{\theta_{11}}$ $= \dfrac{U_e \theta_{11}}{\nu_e}$

r recovery factor

s distance along an external streamline started at a small distance ϵ from the attachment line

s' distance, in chordwise plane, around surface, from the attachment line

s_p' surface distance to velocity maximum (see Fig.1)

S, S_i used in section 2.2.1(c)

T local static temperature

T_0 local total temperature

T_{0_x} total temperature of partial stagnation line (i.e. attachment line) flow $\left(= T_{0_\infty} - \frac{1}{2}U_\infty^2 \cos^2\Lambda/c_p = T_{ref}\right.$ in the Rott[5] transformation - see section 2.2.1(b)$\left.\right)$

NOTATION (continued)

T_r recovery temperature

u velocity in $\underline{U_e}$ direction within the boundary layer

u' velocity in chordwise (s') direction

U_l component of U_e in chordwise direction

U_{l_∞} $= U_\infty \cos \Lambda$

U_e local external velocity

U_τ local friction velocity $\left(= \sqrt{\frac{\tau_w}{\rho_e}} \right)$

v cross-flow velocity, normal to $\underline{U_e}$

v' spanwise velocity

V_e $= V_l = U_\infty \sin \Lambda$

$w_1 \text{---} w_4(n)$ defined in section 2.3.1(d)

Planform coordinate systems:-

x', y', z' rectangular cartesian coordinates with x' chordwise, y' spanwise, z' normal to wing plane

For local boundary layer expressions we use rectangular coordinates with z normal to the surface and either s or s' with the appropriate third normal coordinate direction (y or y')

α angle of incidence

β angle between $\underline{\tau_w}$ and $\underline{U_e}$

γ ratio of specific heats of fluid

δ value of z at which the total velocity within the boundary layer $= 0.995\ U_e$

δ_x 'thickness' of laminar boundary layer in chordwise flow (Ref. Nath[4])

δ_y 'thickness' of laminar boundary layer for spanwise flow

$\bar{\delta}$ $= \int_0^\delta \frac{\rho}{\rho_e}\, dz$

δ^* $= \delta_1^* - \delta_2^* \tan \phi$ (see section 2.3.5)

NOTATION (continued)

$\delta_1^* = \int_0^\delta \left(1 - \frac{\rho u}{\rho_e U_e}\right) dz$,

$\delta_2^* = -\int_0^\delta \frac{\rho v}{\rho_e U_e} dz$

$\delta_1^{*'} = \int_0^\delta \left(1 - \frac{\rho}{\rho_e} \frac{u'}{U_1}\right) dz$, chordwise displacement thickness (Cooke[6])

$\Delta = \delta - \delta^* = \int_0^\delta \frac{\rho u}{\rho_e U_e} dz$

Δs, $\Delta s'$ increments in surface distance for boundary-layer calculations

Δ_{ls} turbulent inner region parameter defined in section 2.3.6

ε distance (s') from attachment line at which boundary layer calculations start

$\lambda \left(= \frac{\theta_x^2}{\nu} \frac{dU_1}{ds'}\right)$ laminar profile shape factor in section 2.2.1(b)

Λ either angle of sweep of wing or laminar profile shape factor $\left(\frac{\delta_x^2}{\nu} \frac{dU_1}{ds'}\right)$ as appropriate. (No ambiguity in the text.)

η transformed z-coordinate for *boundary layer* axes *only*

μ fluid viscosity

$\nu = \frac{\mu}{\rho}$, kinematic viscosity

ρ fluid density

σ' effective leading-edge radius (i.e. the radius of the circular cylinder that, in incompressible flow, has the same velocity gradient as at the attachment line of the aerofoil) of the chordwise section used to find C*

$\pi = \frac{\delta^*}{\tau_{w_1}} \frac{dp}{ds'} \frac{\cos \phi}{\cos \beta}$

τ_w wall shear stress

τ_{w_1} component of wall shear stress in direction of local external velocity (U_e)

NOTATION (continued)

ϕ angle between $\underline{U_e}$ and $\underline{s'}$ vectors

$$\theta_{11} = \int_0^{\delta} \frac{\rho u}{\rho_e U_e}\left(1 - \frac{u}{U_e}\right)dz$$

$$\theta_{12} = \int_0^{\delta} \frac{\rho v}{\rho_e U_e}\left(1 - \frac{u}{U_e}\right)dz$$

$$\theta_{21} = -\int_0^{\delta} \frac{\rho}{\rho_e}\left(\frac{uv}{U_e^2}\right)dz = \theta_{12} + \delta_2^*$$

$$\theta_{22} = -\int_0^{\delta} \left(\frac{v}{U_e}\right)^2 \frac{\rho}{\rho_e}\,dz$$

} conventional definitions based on local streamline coordinates

$$\theta_x = \int_0^{\infty} \left(1 - \frac{u'}{U_1}\right)\frac{\rho}{\rho_e}\frac{u'}{U_1}\,dz$$

$$\theta_{xy} = \int_0^{\infty} \frac{\rho u'}{\rho_e U_1}\left(1 - \frac{v'}{V_1}\right)dz$$

$$\theta_y = \int_0^{\infty} \left(1 - \frac{v'}{V_1}\right)\frac{\rho}{\rho_e}\frac{v'}{V_1}\,dz$$

} notation of Nath[4], for chordwise, spanwise solutions of the laminar layer

$$\theta'_{11} = \int_0^{\delta} \frac{\rho}{\rho_e}\frac{u'}{U_e}\left(\frac{U_1 - u'}{U_e}\right)dz = \frac{U_1^2}{U_e^2}\theta_x$$

$$\theta' = \int_0^{\delta} \frac{\rho}{\rho_e}\frac{u'}{U_e}\left(\frac{V_1 - v'}{U_e}\right)dz = \frac{U_1 V_1}{U_e^2}\theta$$

} notation of Cooke[6] related to that of Ref.4

NOTATION (concluded)

Subscripts:-

a.l.	attachment line value
i	initial value for turbulent flow, or incompressible value in laminar boundary layer transformation. (No ambiguity in text.)
e	value in external potential flow (e.g. U_e)
w	value at surface (e.g. τ_w, ρ_w)
0	stagnation value (e.g. T_0)
T	value in turbulent flow immediately after transition
t.e.	value at the trailing edge
∞	value at infinity upstream
tr	value at the transition position, e.g. $(x'/c')_{tr}$

Superscript:-

'	value using quantities in the x', y', z' coordinate directions, e.g. u', v'

REFERENCES

No.	Author	Title, etc.
1	B.G.J. Thompson G.A. Carr-Hill M. Ralph	The prediction of boundary layer behaviour and profile drag for infinite yawed wings: Part III: Calculations for a particular wing. ARC CP 1309 (1973)
2	B.G.J. Thompson	The prediction of boundary-layer behaviour and profile drag for infinite yawed wings: Part II: Flow near a turbulent attachment line. ARC CP 1308 (1973)
3	B. Thwaites	Approximate calculation of the laminar boundary layer. Aero. Quart., Vol.1, pp.245-280 (1949)
4	G. Nath	The compressible laminar spanwise boundary layer on a yawed infinite cylinder with distributed suction. Acta. Tech. Acad. Sci. Hung., 56 (1-2) pp.187-198 (1966)
5	N. Rott	Compressible laminar boundary layer on a heat-insulated body. J. Aero. Sci., Vol.20, No.1, pp.67-68 (1953)
6	J.C. Cooke	The drag of infinite swept wings, with an Addendum. ARC CP No.1040 (1964)
7	J.F. Nash A.G.J. Macdonald	A turbulent skin-friction law for use at subsonic and transonic speeds. ARC CP No.948 (1966)
8	N.A. Cumpsty M.R. Head	The calculation of three-dimensional turbulent boundary layers. Part II: Attachment-line flow on an infinite swept wing. Aero. Quart., Vol.18, Part II, pp.150-164 (1967)
9	N.A. Cumpsty M.R. Head	The calculation of three-dimensional turbulent boundary layers. Part I: Flow over the rear of an infinite swept wing. Aero. Quart., Vol.18, Part I, pp.55-84 (1967)

REFERENCES (continued)

No.	Author	Title, etc.
10	P.D. Smith	A calculation method for the turbulent boundary layer on an infinite yawed wing in compressible adiabatic flow. ARC CP No.1268 (1972)
11	J.E. Green	The prediction of turbulent boundary-layer development in compressible flow. J.F.M., Vol.31, Part IV, pp.753-778 (1968)
12	J.E. Green	Application of Head's entrainment method to the prediction of turbulent boundary layers and wakes in compressible flow. RAE Technical Report 72079 (ARC 34052) (1972)
13	J.F. Nash J. Osborne A.G.J. Macdonald	A note on the prediction of aerofoil profile drag at subsonic speeds. NPL Aero Report 1196, ARC 28075, June 1966
14	P. Bradshaw	Calculation of three-dimensional turbulent boundary layers. J.F.M., Vol.46, Part III, pp.417-445 (1971)
15	M.R. Head	Entrainment in the turbulent boundary layer. ARC R & M 3152 (1958)
16	K. Stewartson	Correlated incompressible and compressible boundary layers. Proc. Roy. Soc., London, Vol.200, pp.84-100 (1949)
17	N. Rott L.F. Crabtree	Simplified laminar boundary layer calculations for bodies of revolution and for yawed wings. Jour. Aero. Sci., Vol.19, No.8, pp.553-565 (1952)
18	J.F. Nash A.G.J. Macdonald	The calculation of momentum thickness in a turbulent boundary layer at Mach numbers up to unity. ARC CP No.963 (1966)
19	K.G. Winter K.G. Smith J.C. Rotta	Studies of the turbulent boundary layer on a waisted body of revolution in subsonic and supersonic flow. ARC R & M 3633 (1968)

REFERENCES (continued)

No.	Author	Title, etc.
20	B.G.J. Thompson	The prediction of shape-factor development in incompressible turbulent boundary layers with or without transpiration. AGARDograph 97, pp.159-190 (1965)
21	D.B. Spalding S.W. Chi	The drag of a compressible turbulent boundary layer on a smooth flat plate with and without heat transfer. J.F.M., Vol.18, Part I, p.117 (1964)
22	B.G.J. Thompson	A new two-parameter family of mean velocity profiles for incompressible turbulent boundary layers on smooth walls. ARC R & M 3463 (1965)
23	A. Mager	Generalisation of boundary layer momentum integral equations to three-dimensional flows including those of rotating systems. NACA Report 1067 (1952)
24	N.A. Cumpsty M.R. Head	The calculation of three-dimensional turbulent boundary layers. Part III: Comparison of attachment-line calculations with experiment. Aero. Quart., Vol.20, Part II, pp.99-113 (1969)
25	N.A. Cumpsty M.R. Head	The calculation of three-dimensional turbulent boundary layers. Part IV: Comparison of measurement with calculations on the rear of a swept wing. ARC CP No.1077 (1969)
26	P. Wesserling J.P.F. Lindhout	A calculation method for three-dimensional incompressible turbulent boundary layers. Proc. AGARD Conference on turbulent shear flow. London, pp.8.1-8.9
27	J.F. Nash	The calculation of three-dimensional turbulent boundary layers in incompressible flow. J.F.M., Vol.37, Part IV, pp.625-642 (1969)

REFERENCES (continued)

No.	Author	Title, etc.
28	R.S. Crabbe	Measurements in a laterally strained turbulent boundary layer. McGill University Report 71-2, February 1971
29	D.F. Myring	An integral prediction method for three-dimensional turbulent boundary layers in incompressible flow. RAE Technical Report 70147 (ARC 32647) (1970)
30	G.S. Raetz	A method of calculating three-dimensional laminar boundary layers of steady compressible flows. Report NAI-58-73 (BLC-114), Northrop Corp. (1957) Also ARC 23634 (1962)
31	M.J. Lighthill	On displacement thickness. J.F.M., Vol.4, Part IV, pp.383 (1958)
32	J.C. Cooke	Boundary layers over infinite yawed wings. Aero. Quart., Vol.9, p.333 (1960)
33	V.C. Patel	Calibration of the Preston tube and limitations of its use in pressure gradients. J.F.M., Vol.23, pp.185-208 (1965)
34	P.D. Chappell M.D. Hodges	Note on the effect of wake treatment on profile drag predictions using the J.F. Nash boundary-layer development. ESDU A150 (1967)
35	D.J. Hall V.G. Quincey R.C. Lock	Some results of wind tunnel tests on an aerofoil section (NPL 9510) combining a 'peaky' upper surface pressure distribution with rear loading. ARC CP No.1292 (1969)
36	M.G. Hall	A numerical method for calculating steady three-dimensional laminar boundary layers. RAE Technical Report 67145 (ARC 29525) (1967)
37	J.E. Green D.J. Weeks J.W.F. Brooman	Prediction of turbulent boundary layers and wakes in compressible flow by a lag-entrainment method. RAE Technical Report 72231 (ARC 34458) (1973)

REFERENCES (concluded)

No.	Author	Title, etc.
38	B.G.J. Thompson G.A. Carr-Hill B.J. Powell	A programme of research into the viscous aspects of flow on swept wings. NPL Aero Note 1100, ARC 32402 (1970)

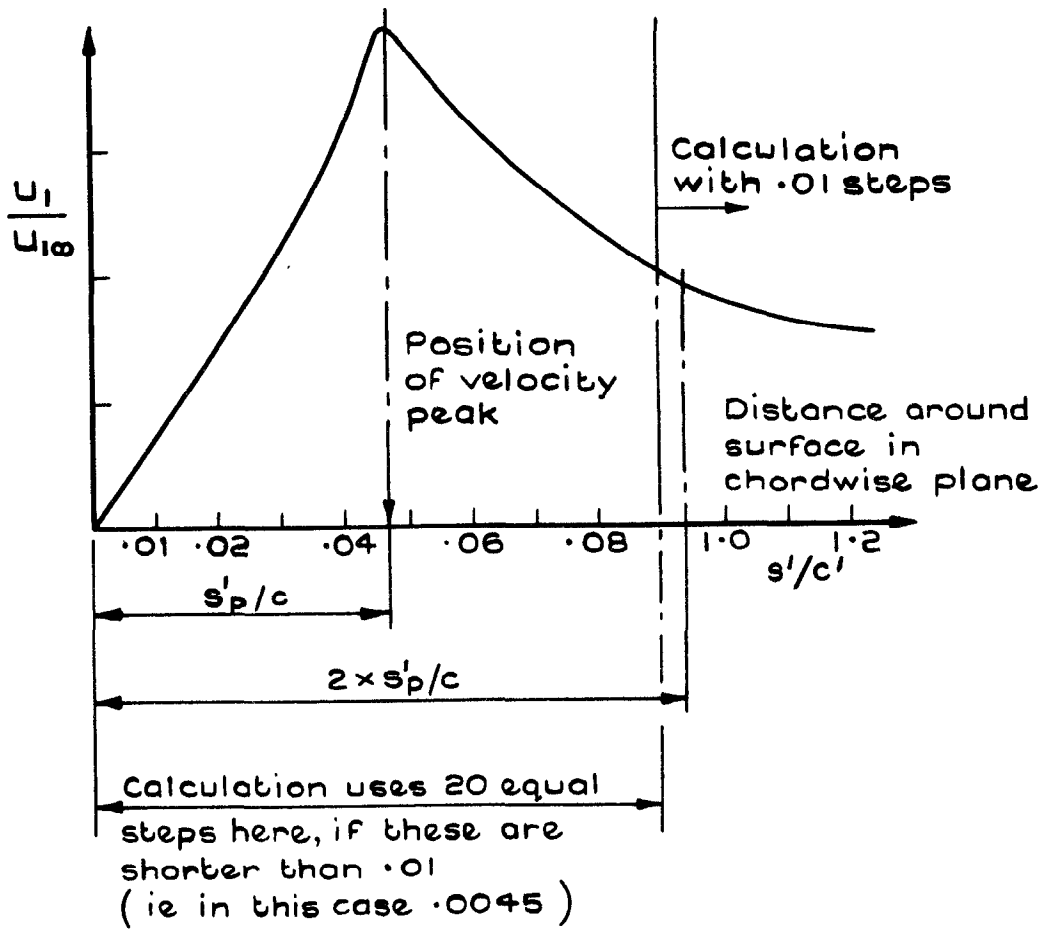

Fig.1 Sketch explaining step length control applied near velocity peak

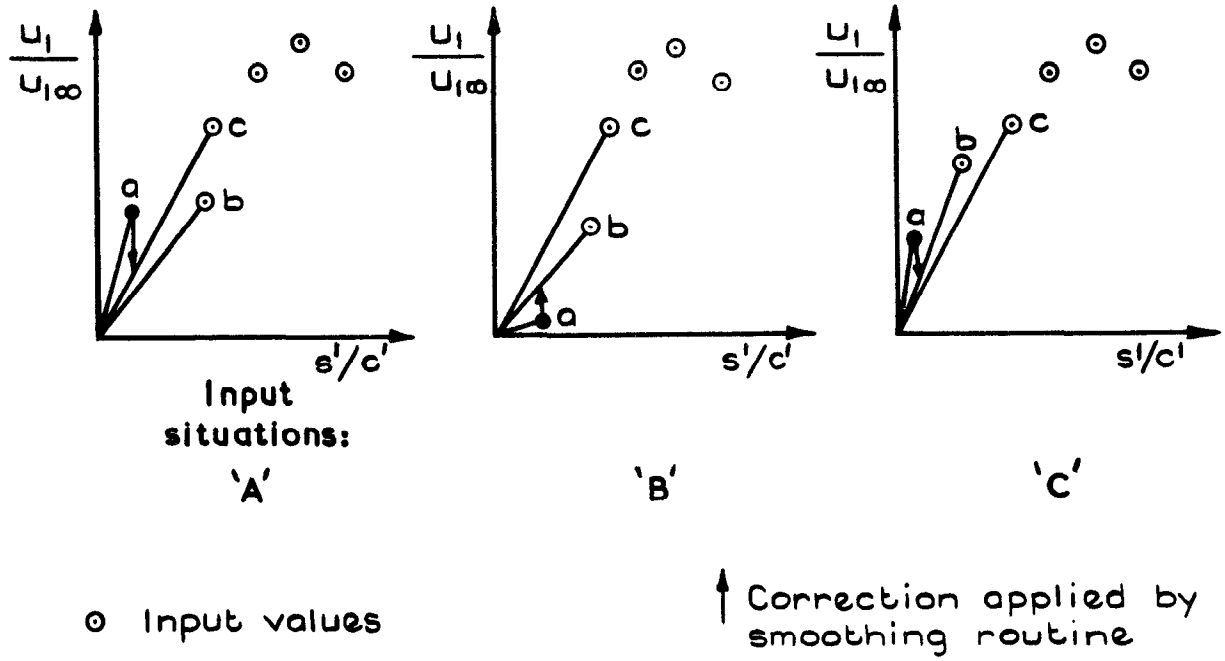

Fig.2 Sketches to explain smoothing of input near to a leading edge attachment line

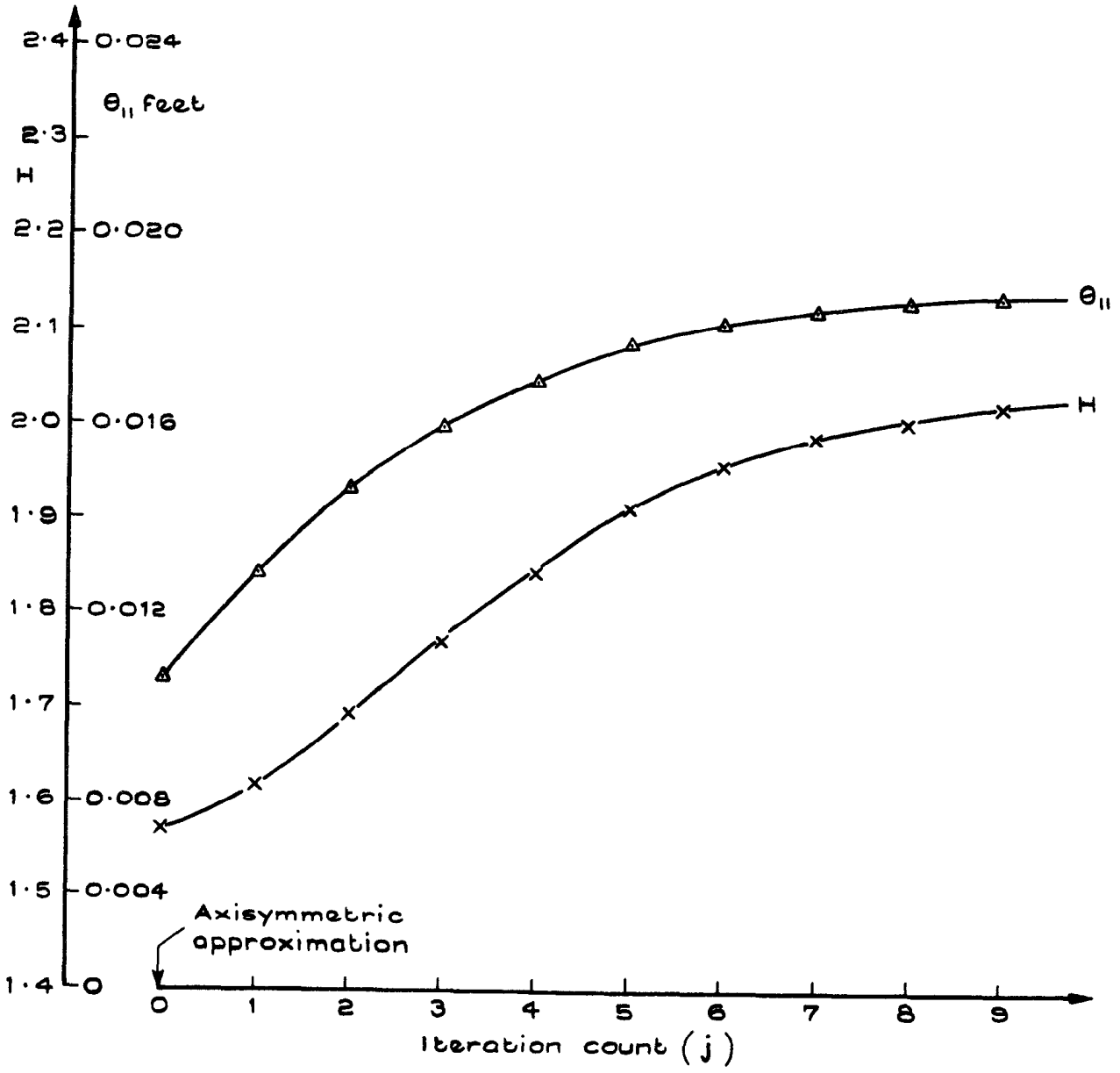

Fig.3 Slow convergence of global iteration method close to rear separation.

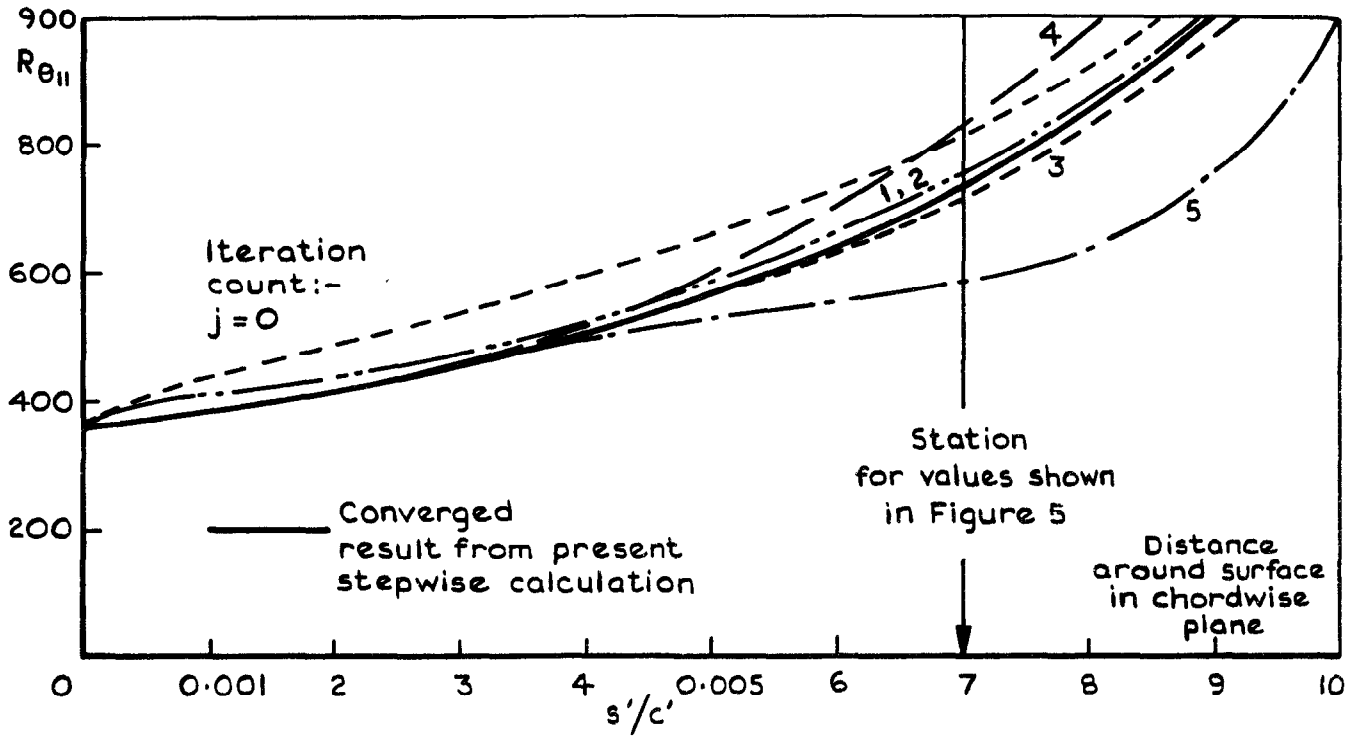

Fig.4 Successive iterations using a value of damping parameter, P=0·2

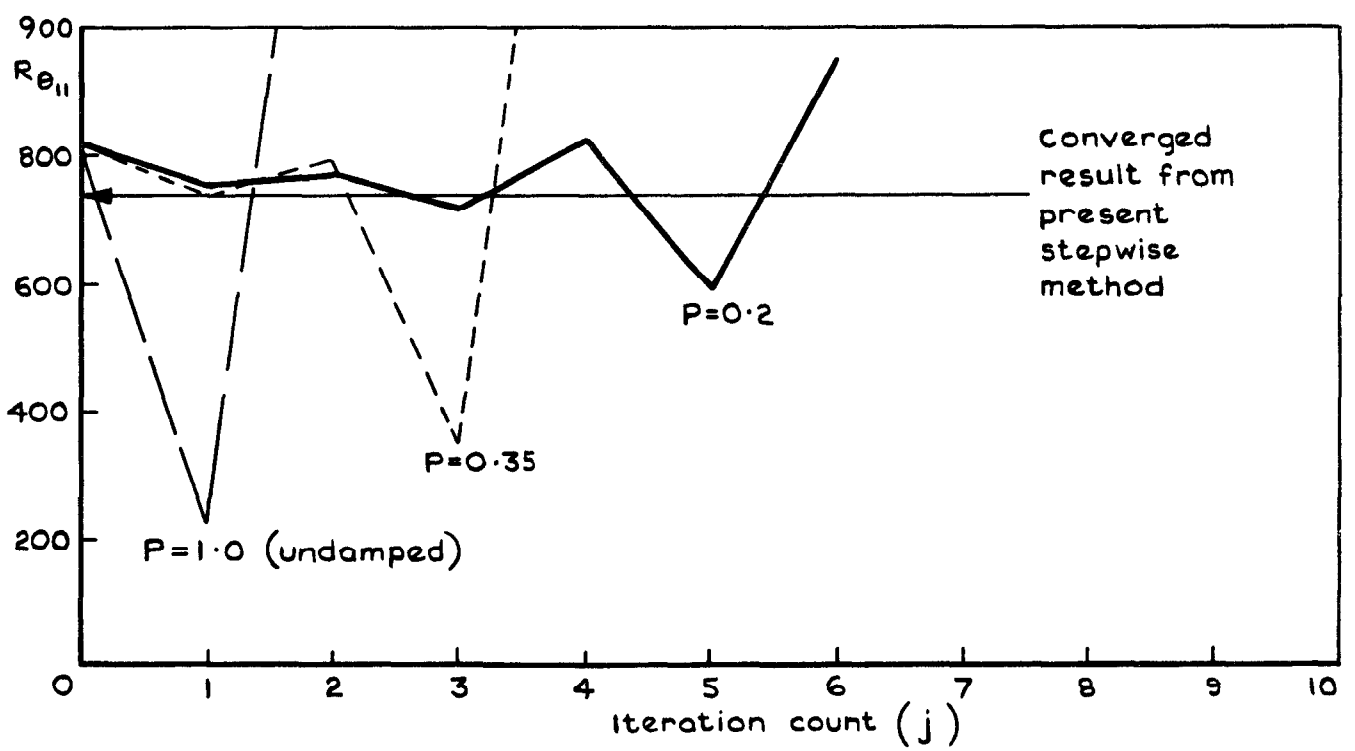

Fig.5 Effect of damping, at s'/c = 0·007.
Typical behaviour of global iteration method[9] in favourable pressure gradients close to a leading edge

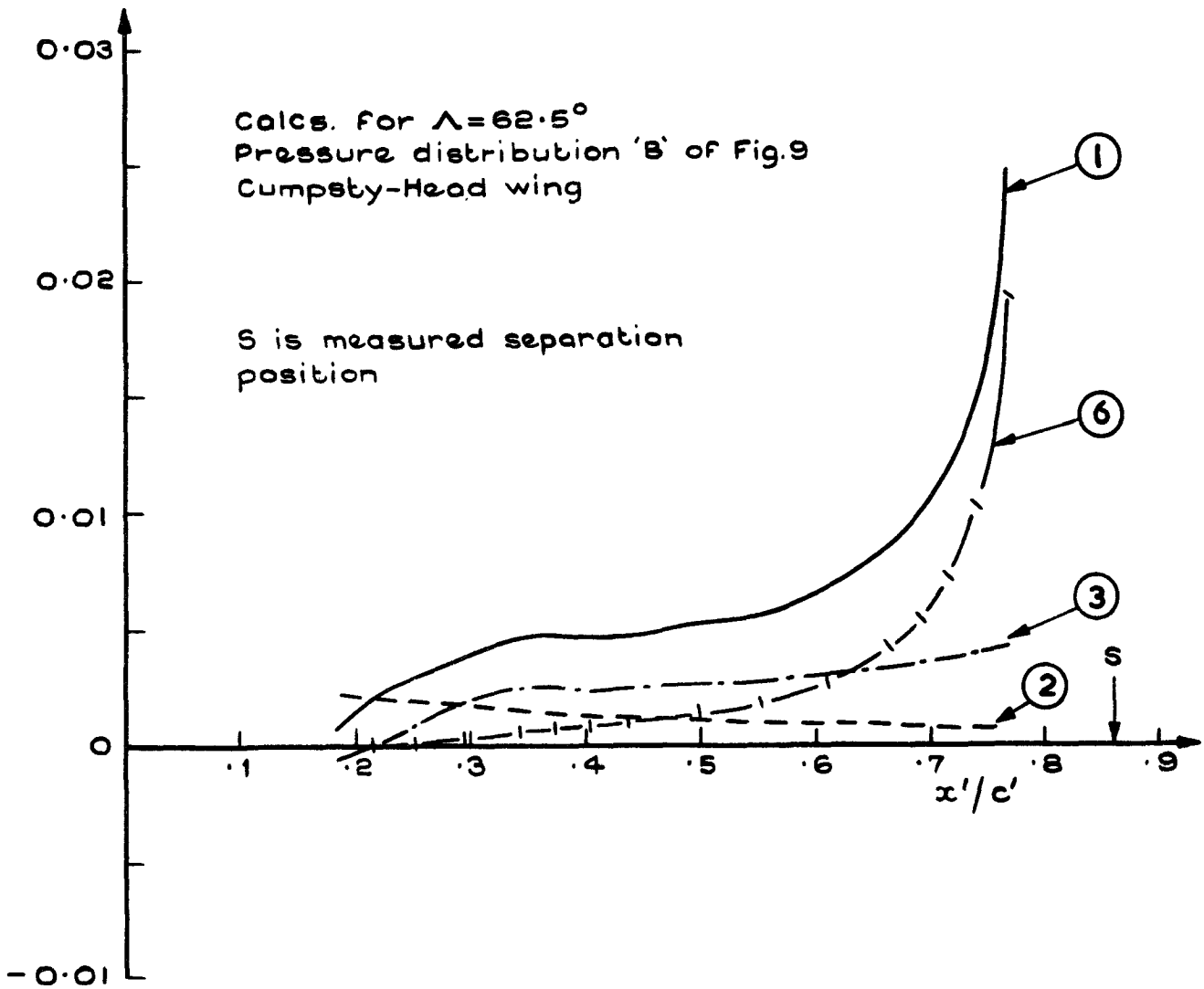

Fig.6a Comparison of terms in the streamwise momentum integral equation

$$\frac{d\theta_{11}/c}{ds/c} = \frac{C_{f_1}}{2} + \frac{\theta_{11}}{c}\left[K_1 c - (H+2-M_e^2)\,\frac{1}{U_e}\frac{dU_e}{ds/c}\right]$$

① ② ③

$$-K_1 c\,\frac{\theta_{22}}{c} - \frac{\theta_{12}}{c}\left[M_e^2 \tan\phi\,\frac{1}{U_e}\,\frac{dU_e}{ds/c}\right] + \frac{d\theta_{12}/c}{ds/c}\tan\phi$$

④ ⑤ ⑥

$$\{\text{Terms } ④ \text{ and } ⑤ < 10^{-4}\}$$

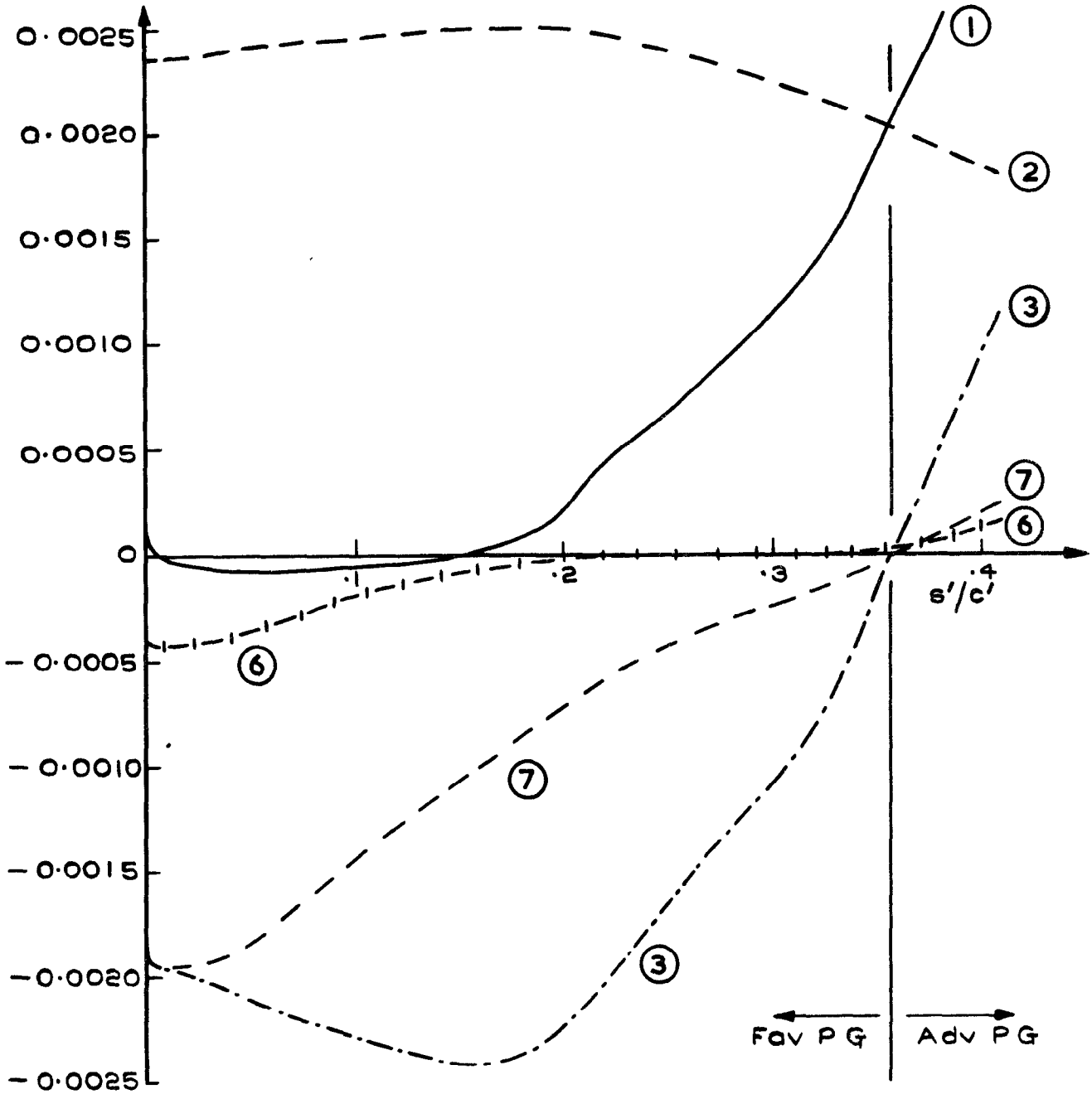

Fig. 6b Comparison of terms in the streamwise momentum equation for the leading edge region

$$\frac{d\theta_{11}/c}{ds/c} = \frac{Cf_1}{2} + \frac{\theta_{11}}{c}\left[K_1 c - (H+2-M_e^2)\frac{1}{U_e}\frac{dU_e}{ds/c}\right]$$

① ② ③

$$-K_1 c\,\frac{\theta_{22}}{c} - \frac{\theta_{12}}{c}\left[M_e^2 \tan\phi\,\frac{1}{U_e}\,\frac{dU_e}{ds/c}\right] + \frac{d\theta_{12}/c}{ds/c}\tan\phi$$

④ ⑤ ⑥

$$\left\{\text{Term } ⑦ \text{ is } c\,K_1\,\theta_{11}/c\right\}$$

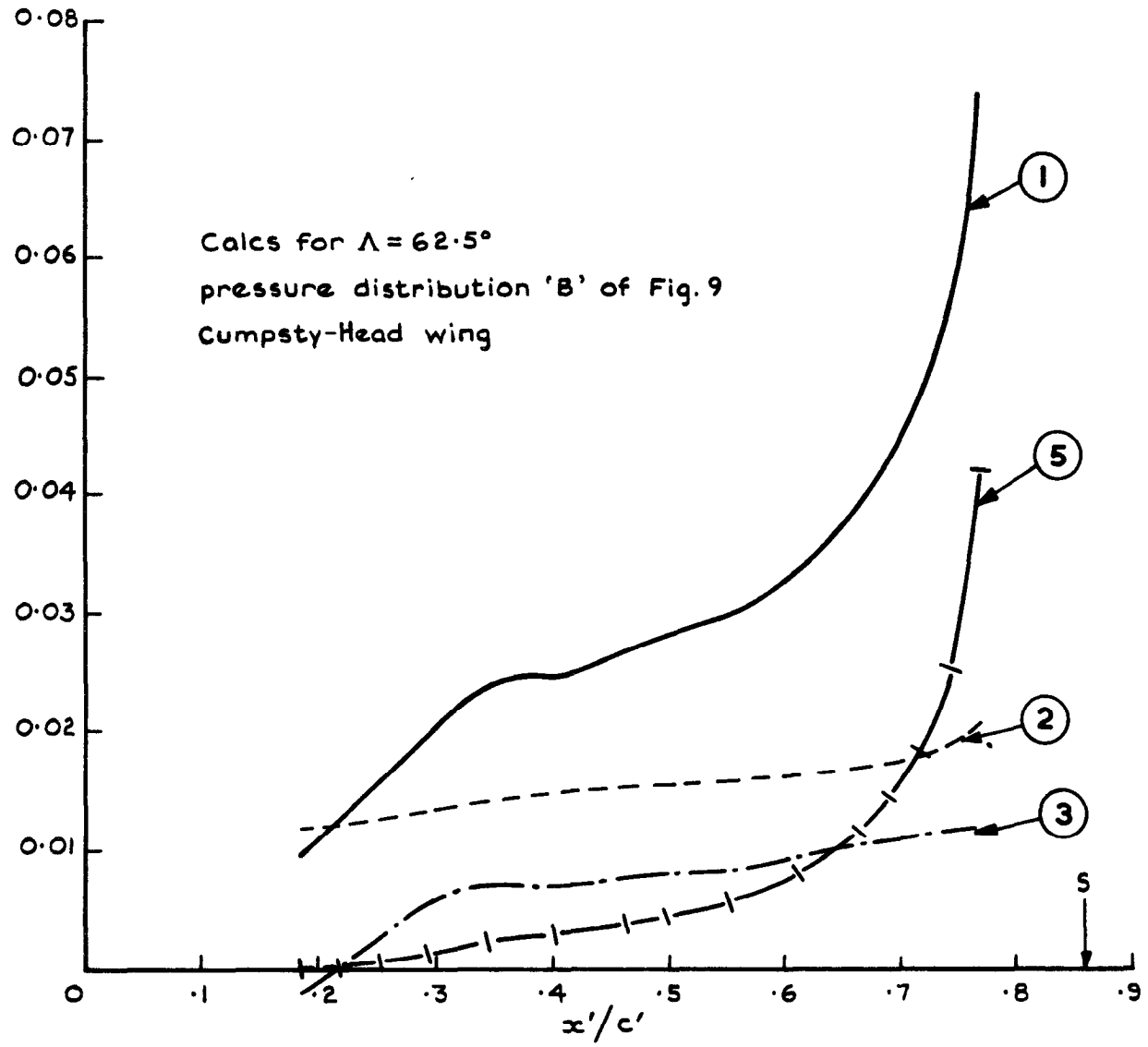

Fig 7a Comparison of terms in the entrainment equation

$$\frac{d\Delta/c}{d^s/c} = F(H_1) - \Delta/c \left[(1 - M_e^2) \frac{1}{U_e} \frac{dU_e}{d^s/c} - K_1 c \right]$$

① ② ③

$$+ \frac{\delta_2^*}{c} \left[\frac{M_e^2}{U_e} \frac{dU_e}{d^s/c} \tan \phi \right] - \frac{d\delta_{2/c}^*}{d^s/c} \tan \phi$$

④ ⑤

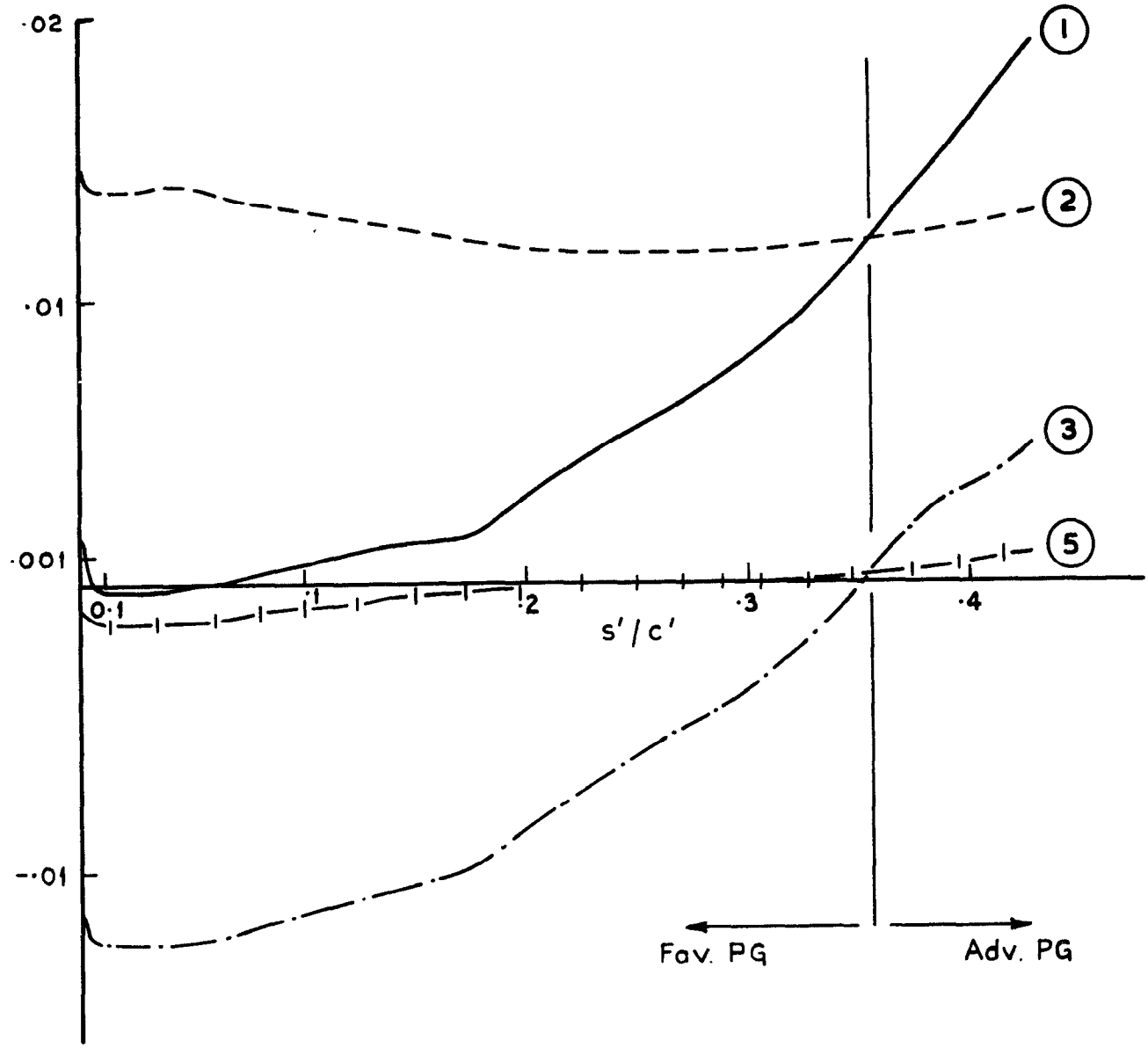

Fig. 7b Comparison of terms in the entrainment equation for the leading edge region

$$\frac{d\Lambda_1/c}{ds/c} = F(H_1) - \Lambda_1/c\left[(1-M_e^2)\frac{1}{U_e}\frac{dU_e}{ds/c} - K_1 c\right]$$

① ② ③

$$+ \frac{\delta_2^*}{c}\left[\frac{M_e^2}{U_e}\frac{dU_e}{ds/c}\tan\phi\right] - \frac{d\delta_{2/c}^*}{ds/c}\tan\phi$$

④ ⑤

$$\left\{\text{Term } ④ < 10^{-5}\right\}$$

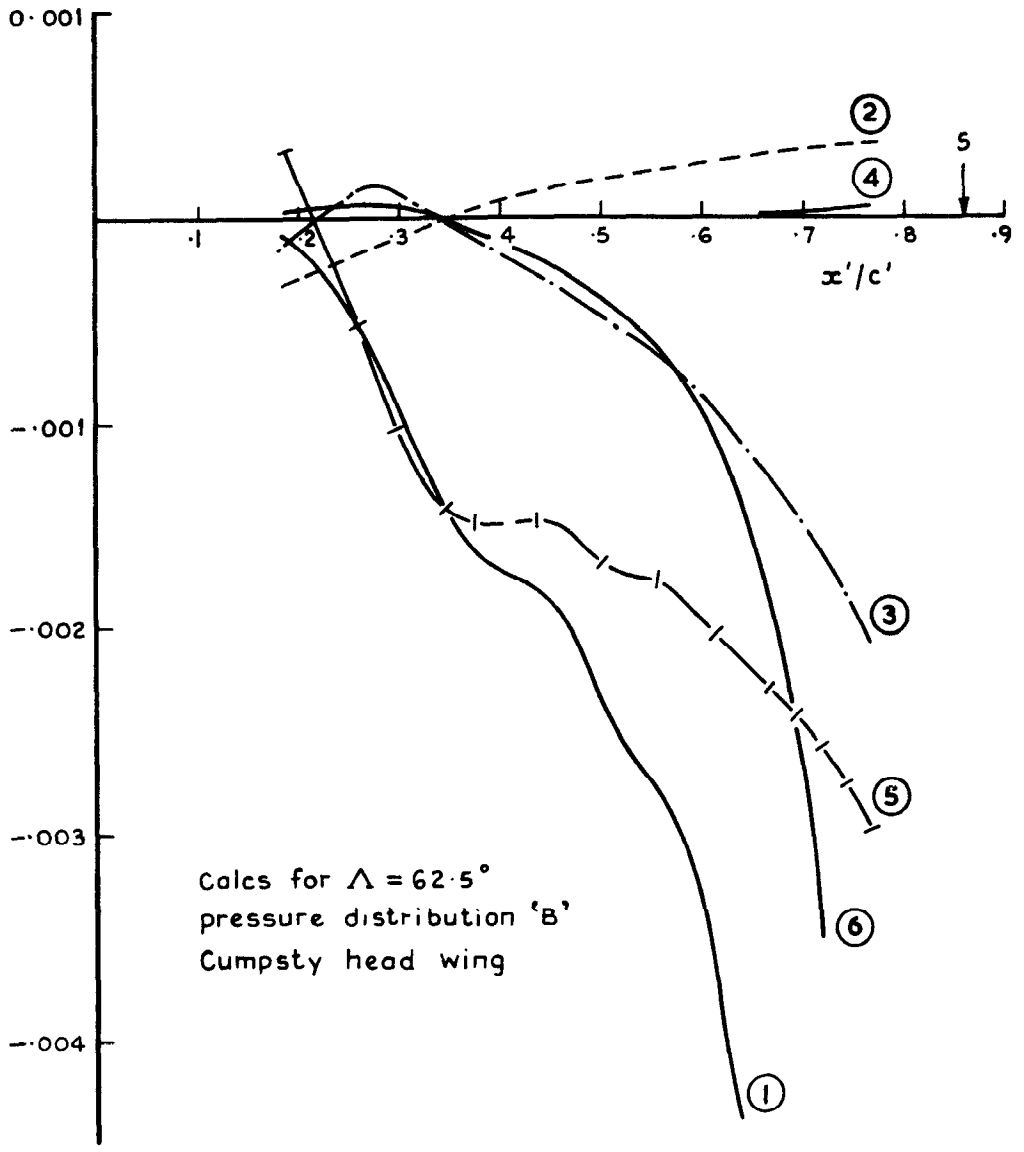

Fig. 8a Comparison of terms in the crossflow momentum equation

$$\frac{d\theta_{12/c}}{d^s/c} = \frac{C_{f_i}\ \tan\beta}{2} + \frac{\theta_{12}}{c}\left[2K_1 c + \left(M_e^2 - 2\right)\frac{1}{U_e}\frac{dU_e}{d^s/c}\right]$$

① ② ③

$$+ \frac{\theta_{22}}{c}\left[1-M_e^2\right]\frac{\tan\phi}{U_e}\frac{dU_e}{d^s/c} + \frac{\theta_{11}}{c}(1+H)\frac{\tan\phi}{U_e}\frac{dU_e}{d^s/c} + \tan\phi\ \frac{d\theta_{22/c}}{d^s/c}$$

④ ⑤ ⑥

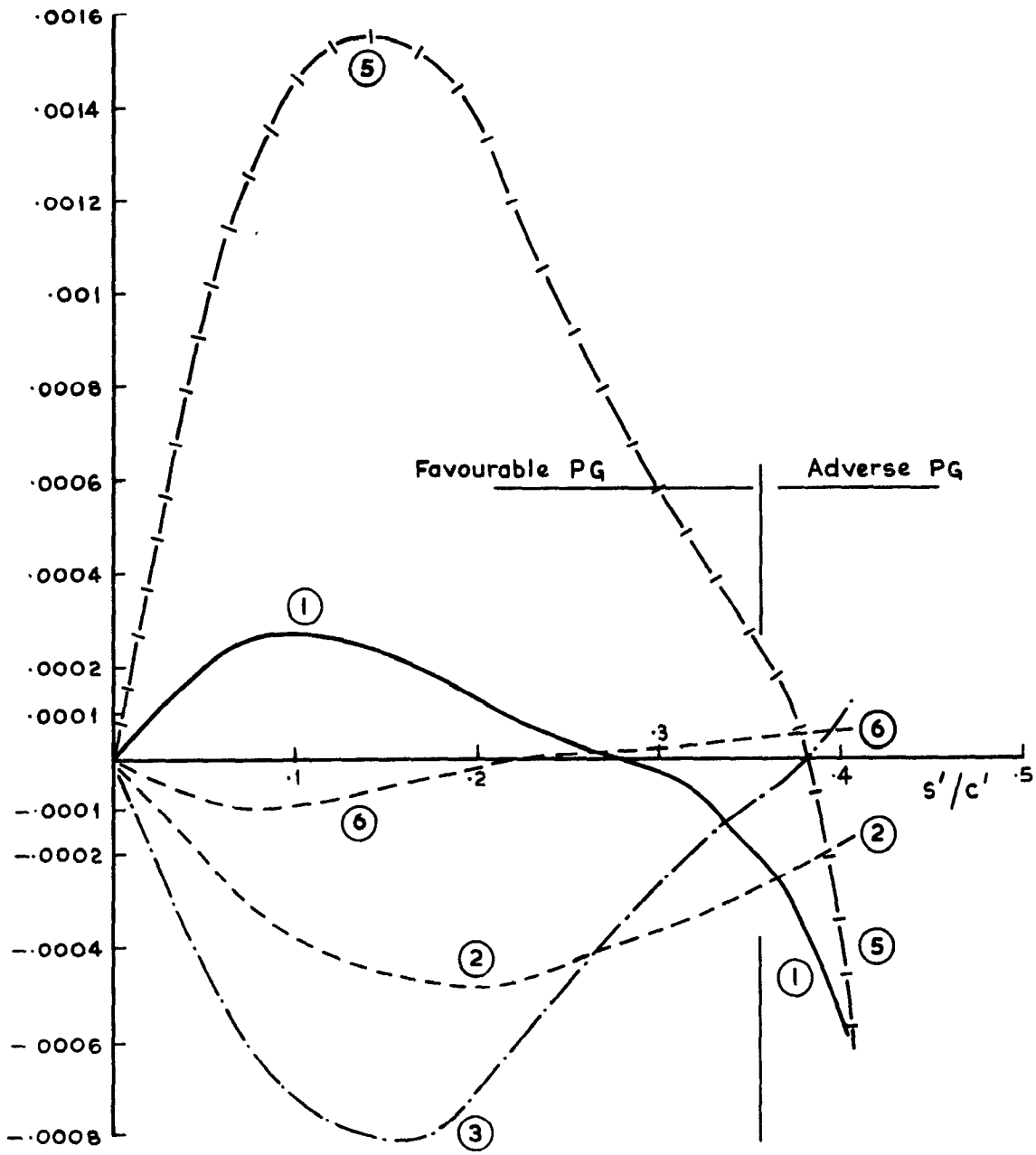

Fig. 8b Comparison of terms in the crossflow momentum equation for the leading edge region

$$\frac{d\theta_{12/c}}{d^{s}/_{c}} = \frac{C_{f_1}\tan\beta}{2} + \frac{\theta_{12}}{c}\left[2K_1 c + \left(M_e^2 - 2\right)\frac{1}{U_e}\frac{dU_e}{d^{s}/_{c}}\right]$$

① ② ③

$$+ \frac{\theta_{22}}{c}\left[1-M_e^2\right]\frac{\tan\phi}{U_e}\frac{dU_e}{d^{s}/_{c}} + \frac{\theta_{11}}{c}\left(1+H\right)\frac{\tan\phi}{U_e}\frac{dU_e}{d^{s}/_{c}} + \tan\phi\,\frac{d\theta_{22/c}}{d^{s}/_{c}}$$

④ ⑤ ⑥

$$\left\{\text{Term } ④ < 10^{-5}\right\}$$

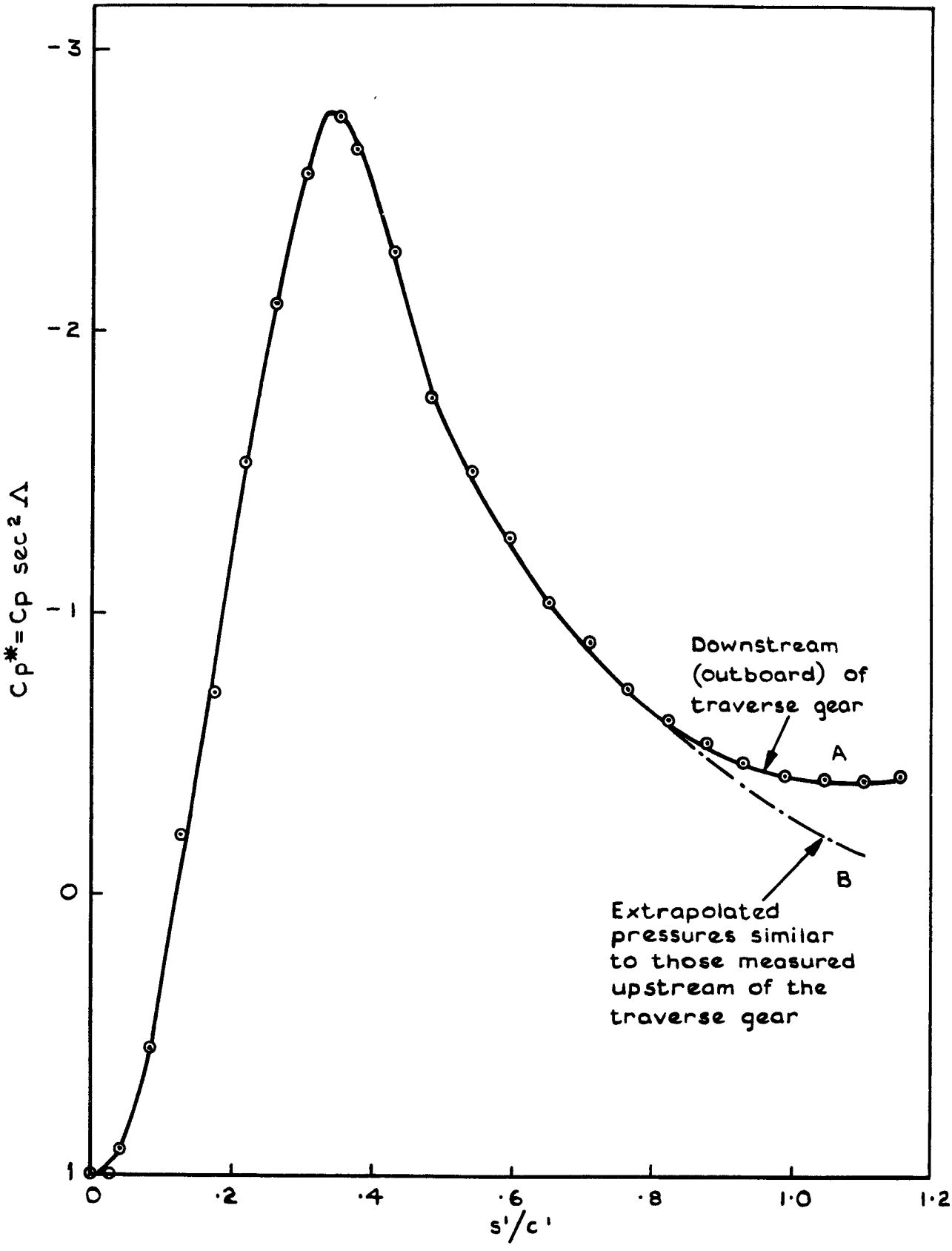
-3
-2
-1
0
1
$C_p^* = C_p \sec^2 \Lambda$
0
·2
·4
·6
·8
1·0
1·2
s'/c'
Downstream (outboard) of traverse gear
A
B
Extrapolated pressures similar to those measured upstream of the traverse gear

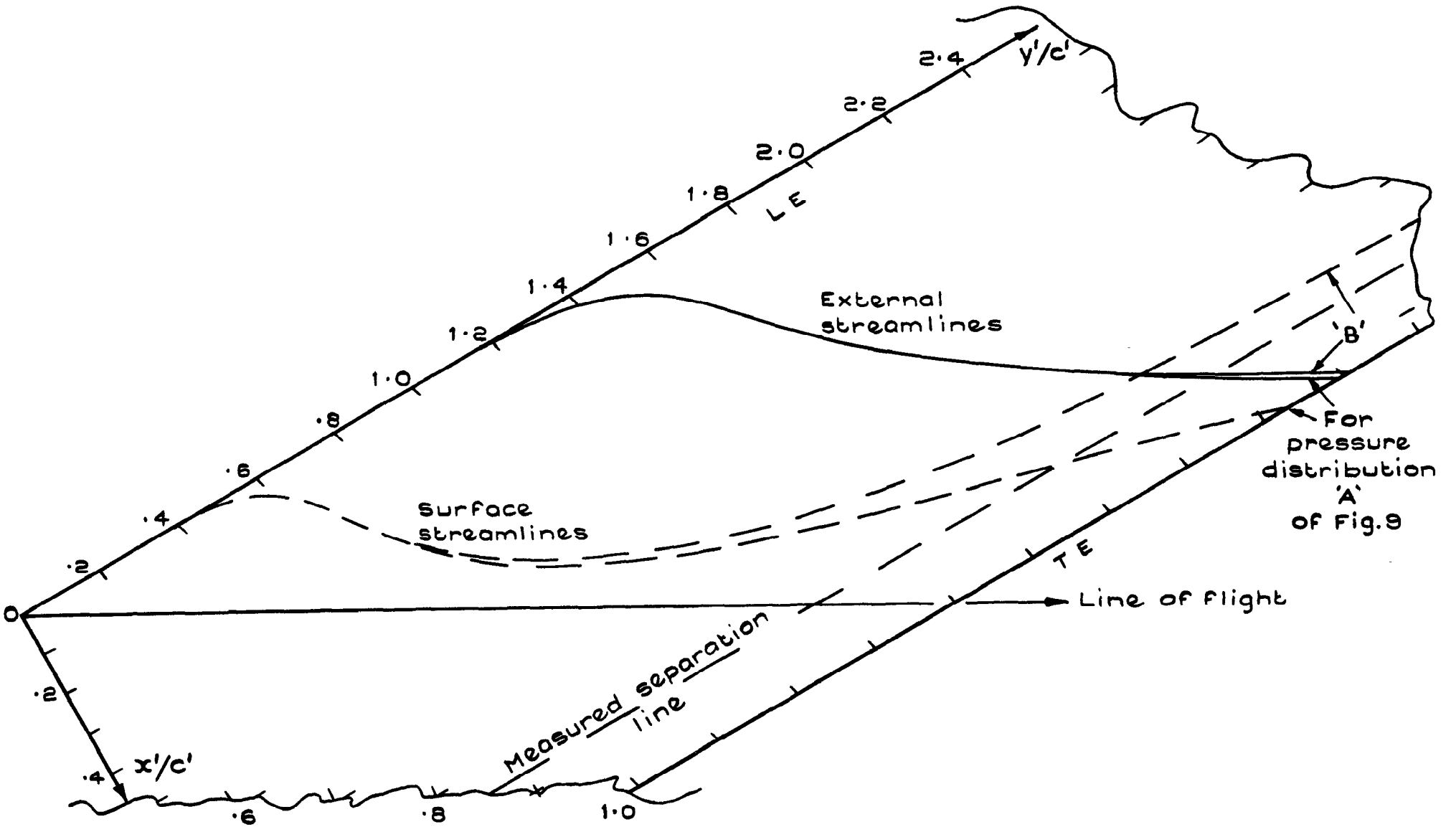

Fig.10 Calculated streamlines for Cumpsty 62·5° wing

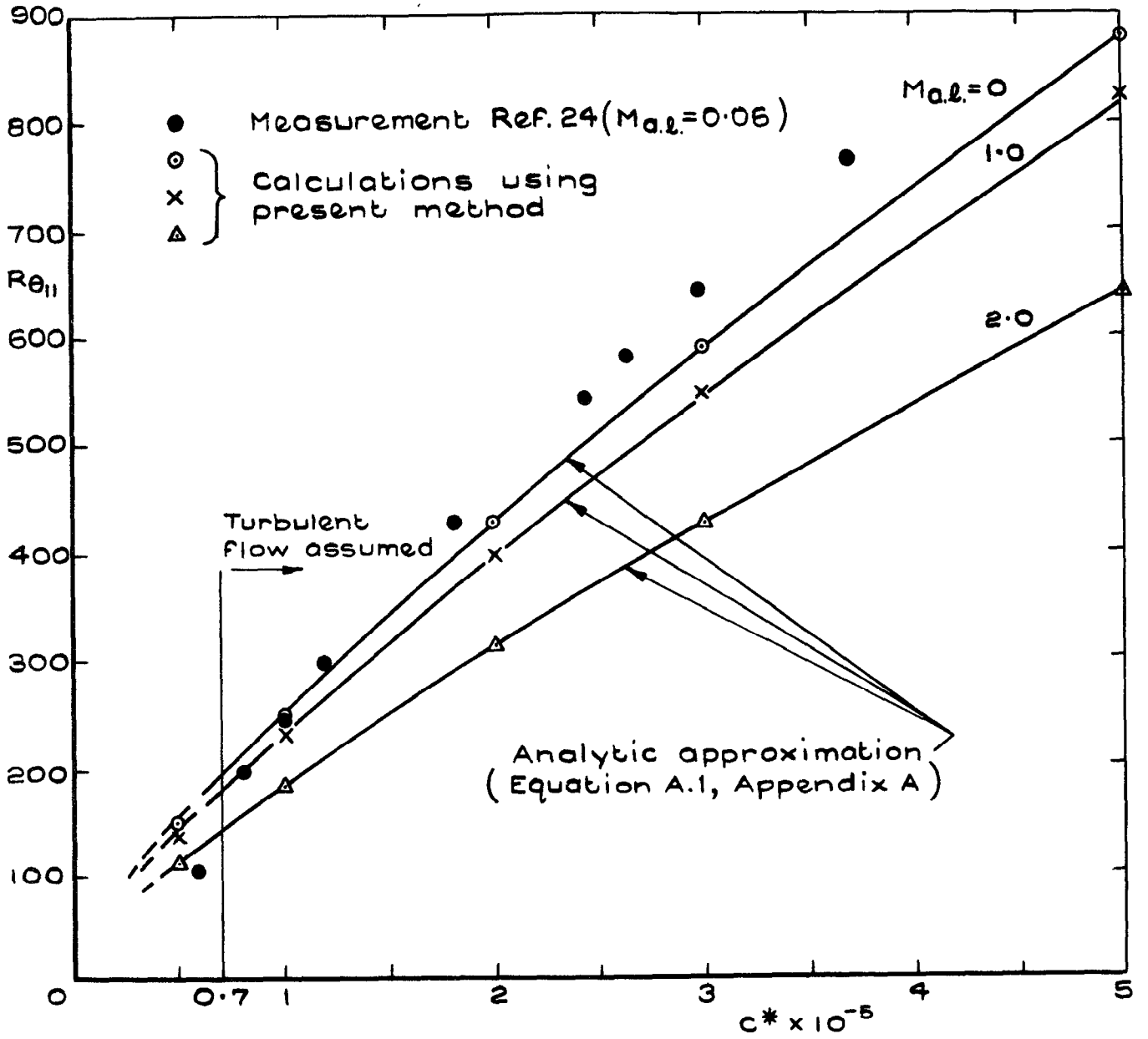

Fig. 11 Extension to compressible flow, of the Cumpsty calculations for the turbulent boundary layer on the attachment line of infinite yawed wings

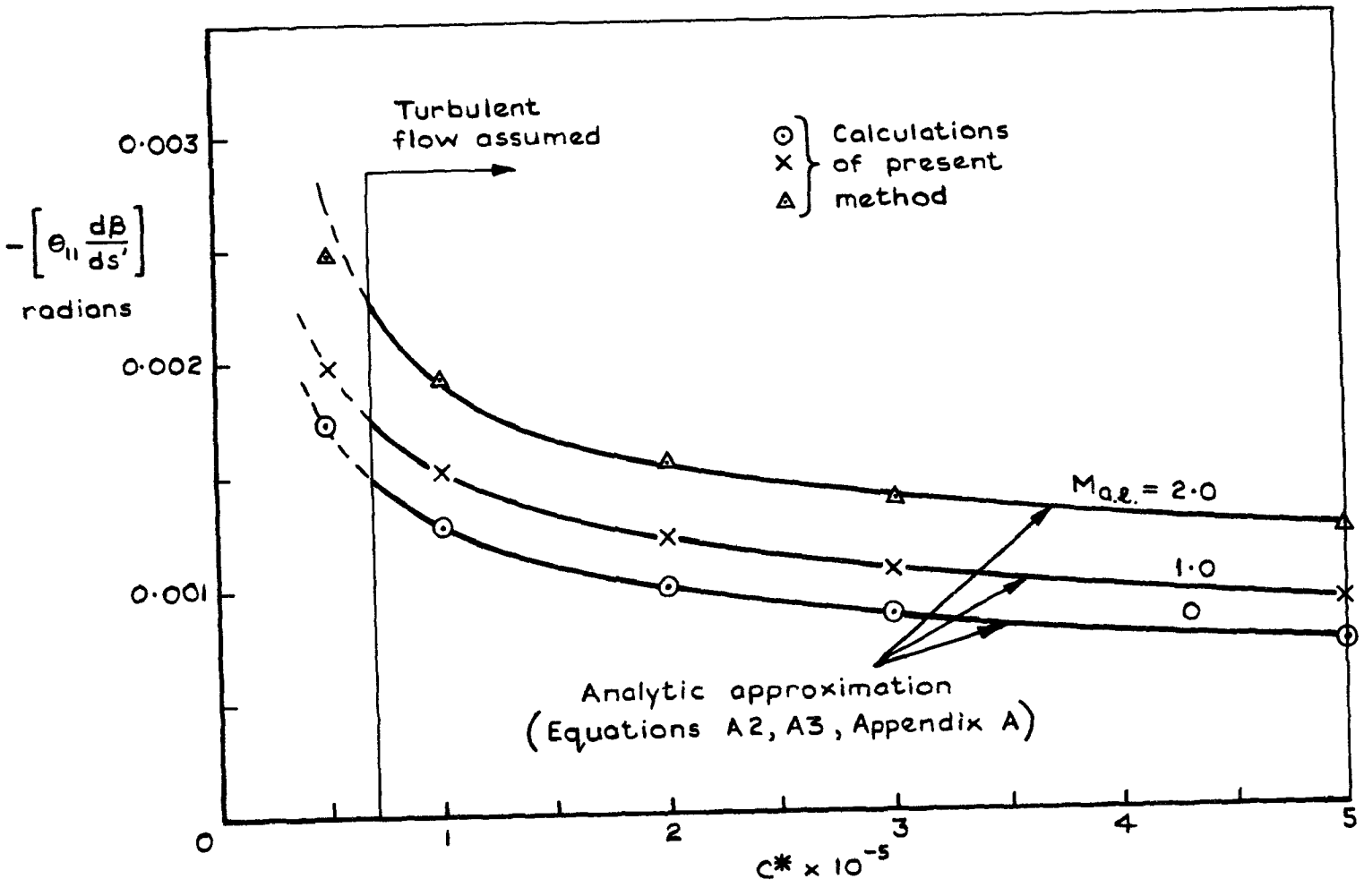

Fig. 12 Compressible turbulent attachment line flow (cont)

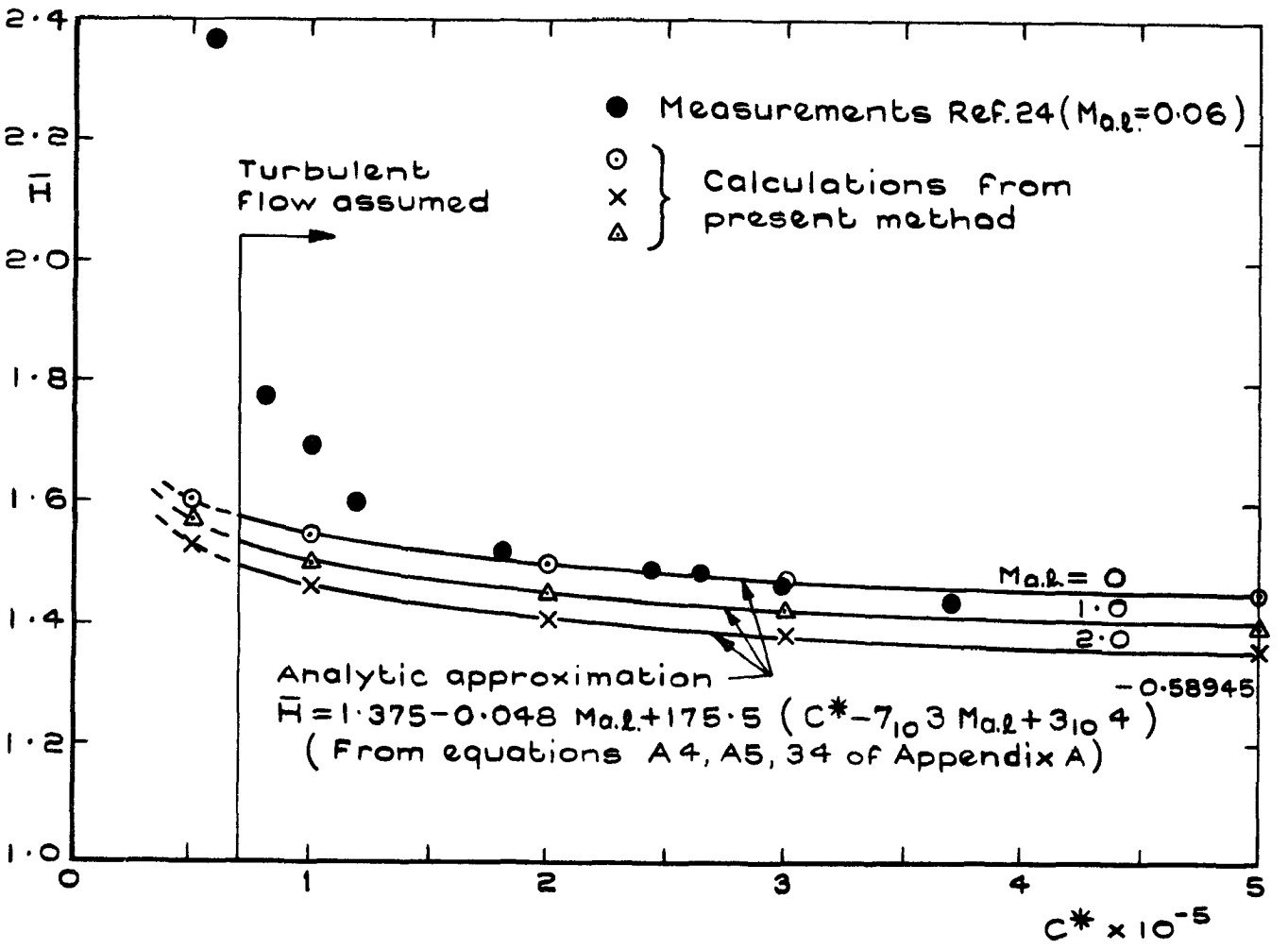
2·4
2·2
2·0
1·8
1·6
1·4
1·2
1·0
H̄
0
1
2
3
4
5
C* x 10⁻⁵
Measurements Ref.24 (Ma.ℓ=0·06)
Calculations from present method
Turbulent flow assumed
Ma.ℓ= 0
1·0
2·0
Analytic approximation
H̄ = 1·375 − 0·048 Ma.ℓ + 175·5 (C* − 7₁₀3 Ma.ℓ + 3₁₀4)
− 0·58945
(From equations A4, A5, 34 of Appendix A)

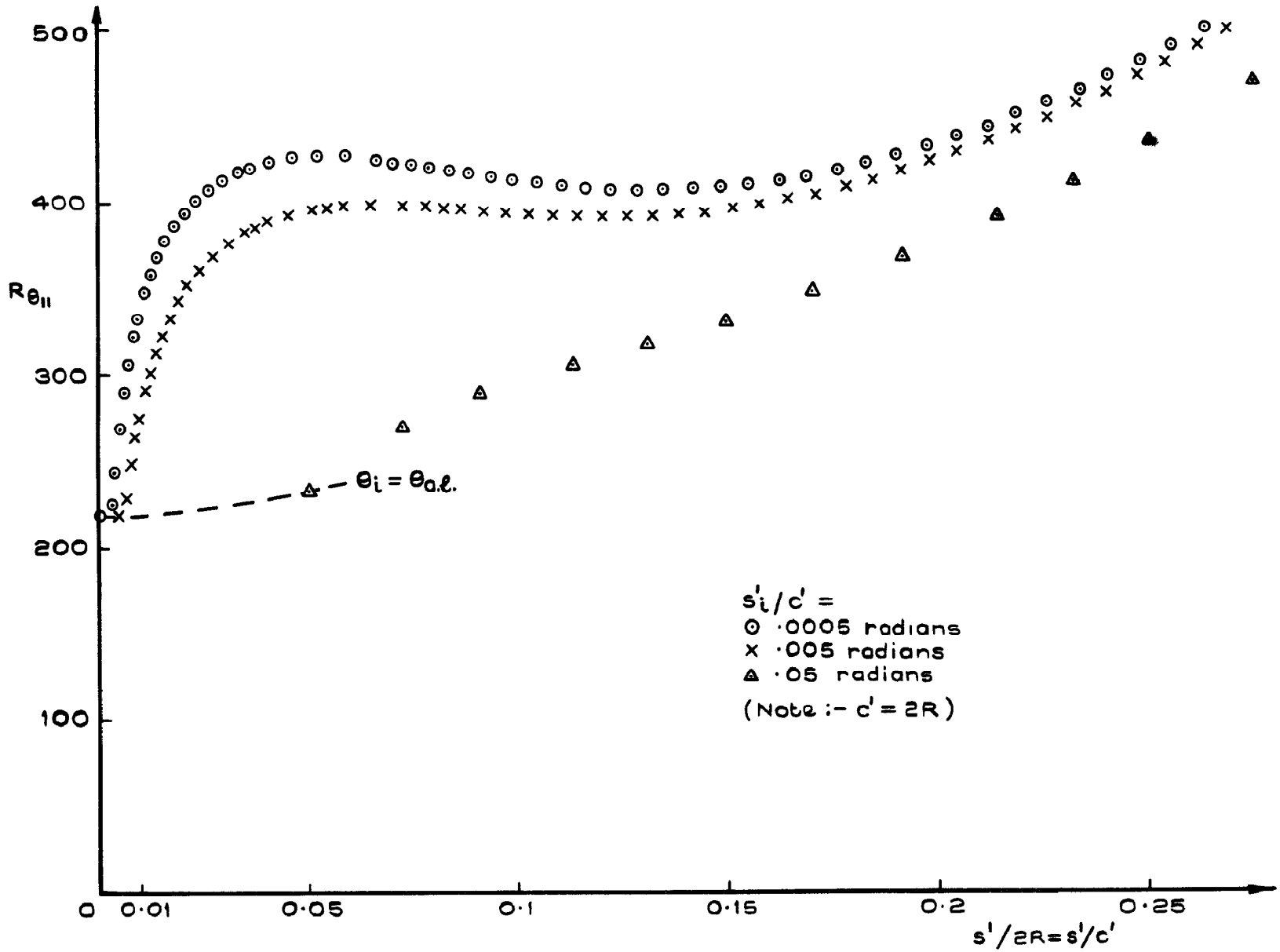

Fig.14 Effect of initial values upon boundary layer development just downstream of swept attachment line of a yawed circular cylinder

$R_{c'} = 1 \times 10^6$, $\Lambda = 30^\circ$, $C^* = 8{\cdot}33 \times 10^{-4}$, $M_{a.\ell.} = 0{\cdot}01$

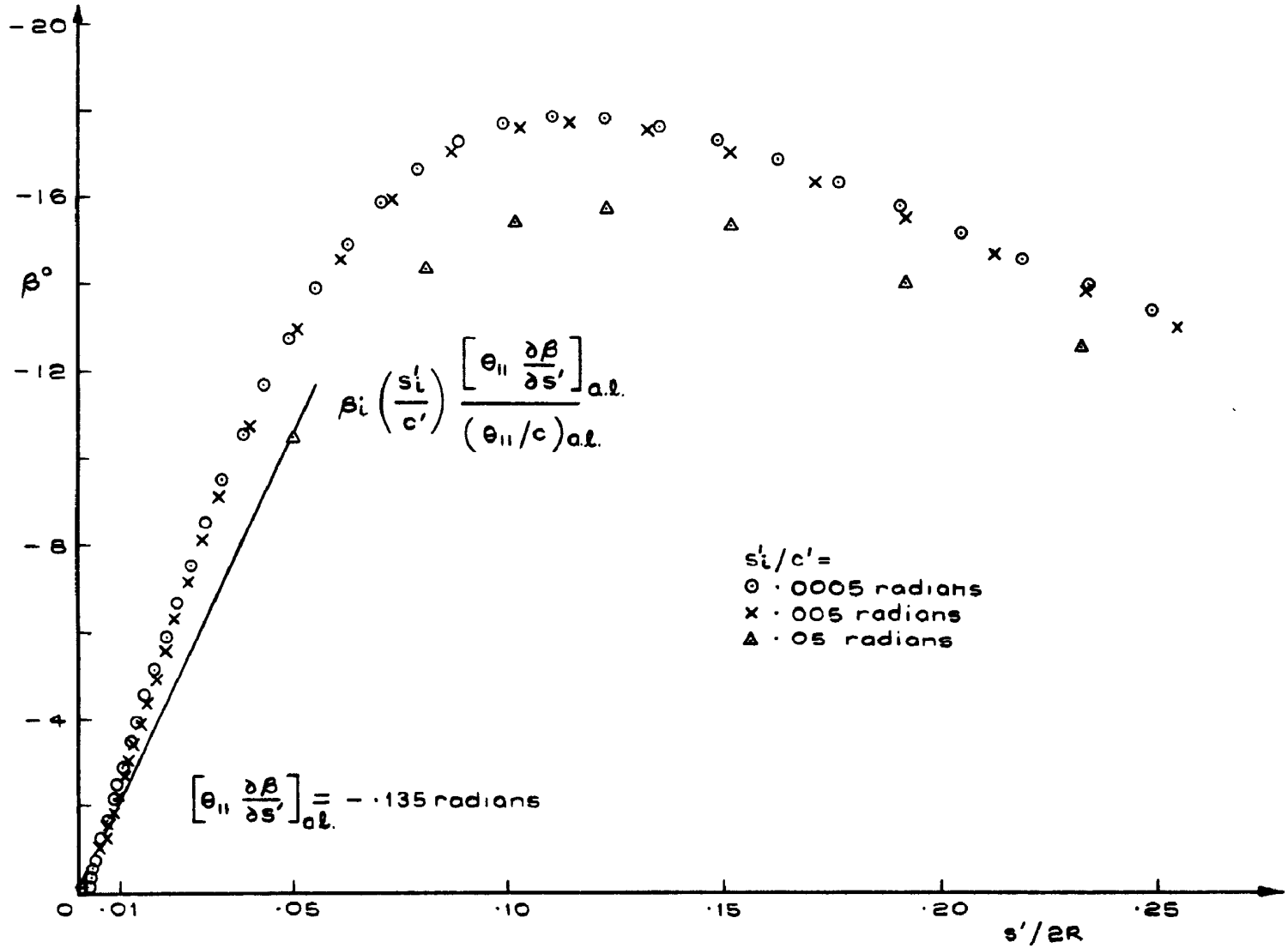

Fig.15 Effect of initial values on development of crossflow

(Conditions of Fig.14)

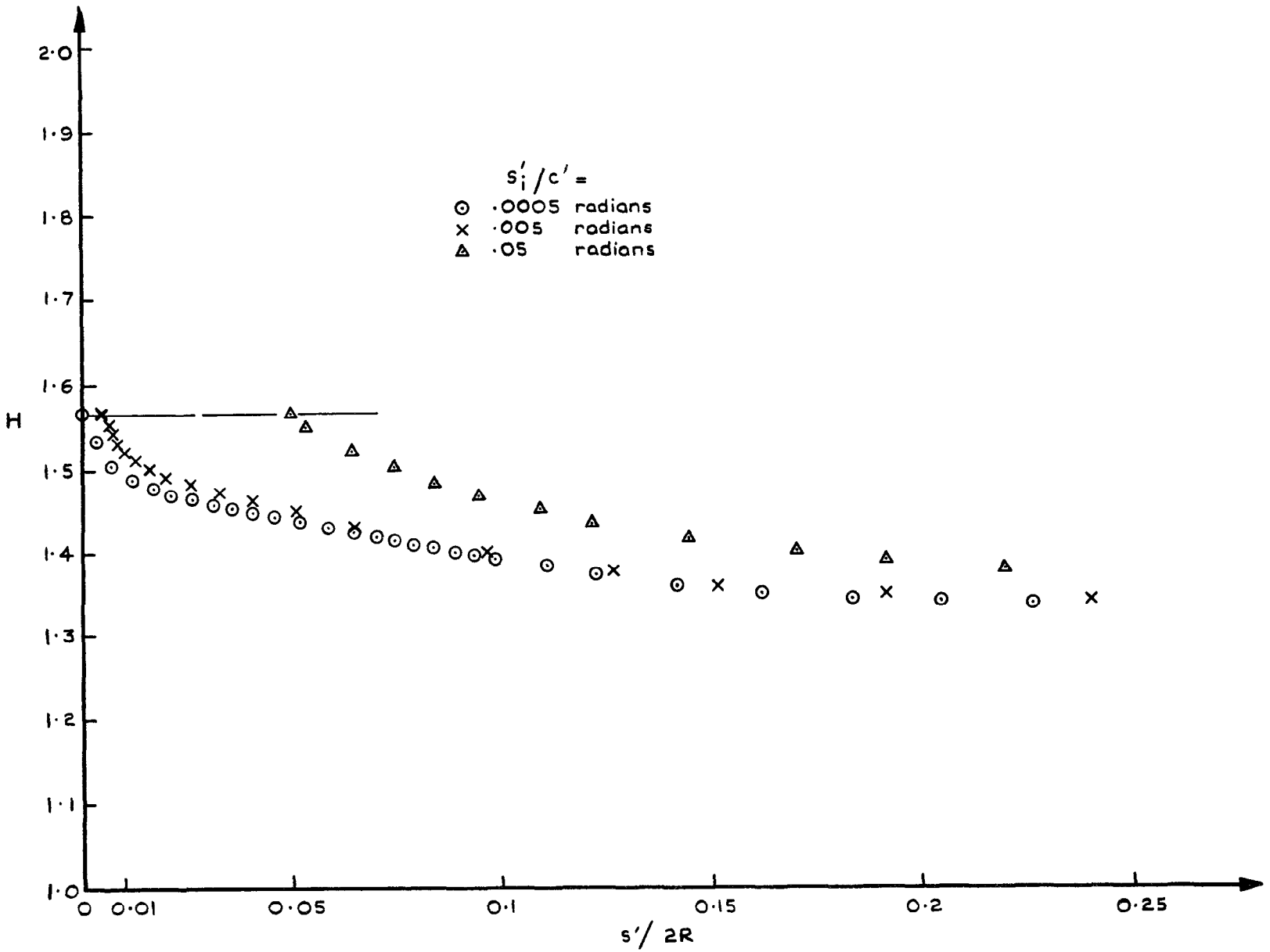

Fig. 16 Effect of initial conditions on the development of shape factor
(Conditions of Fig. 14)

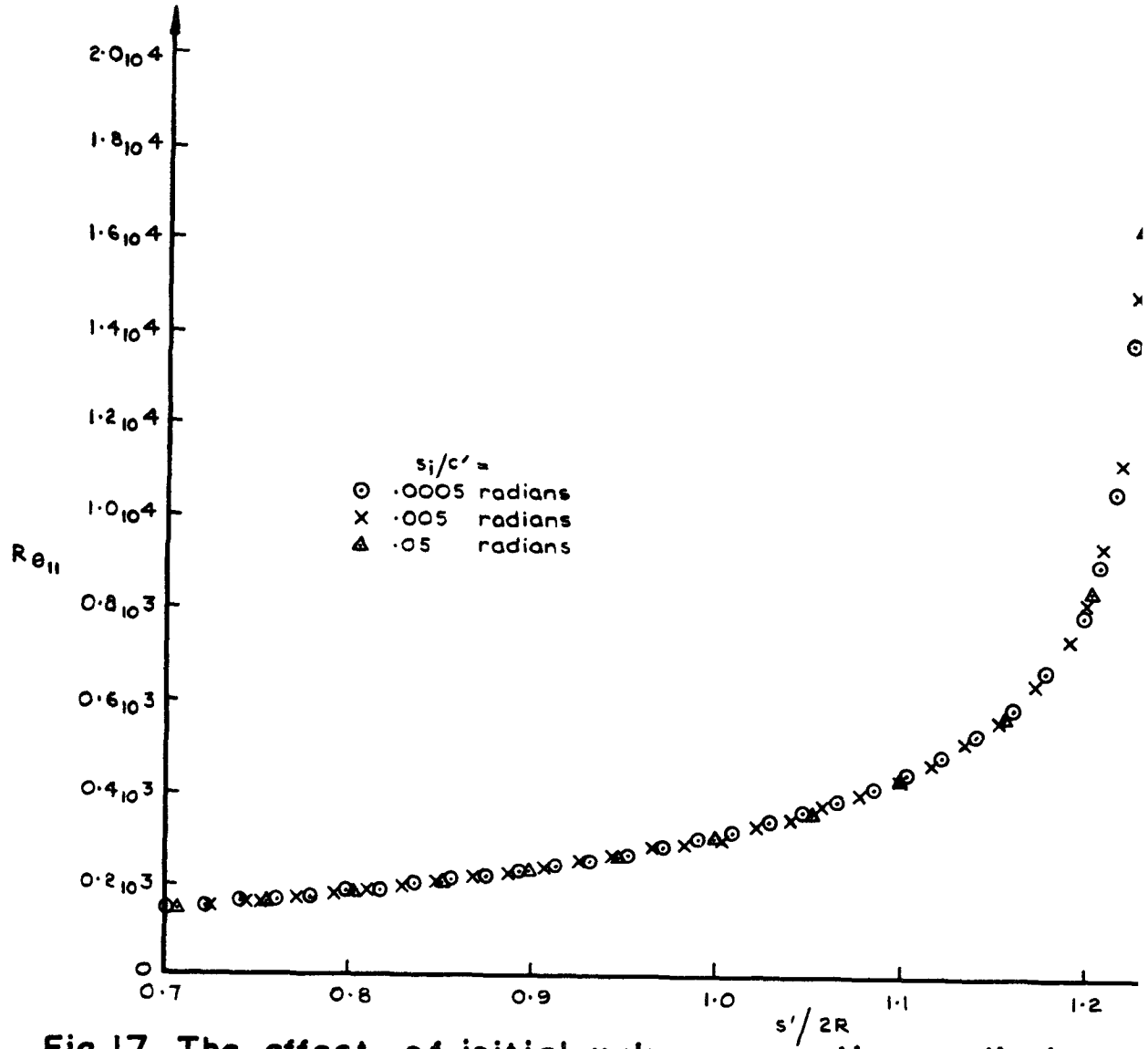

Fig. 17 The effect of initial values upon the prediction of development up to separation, for a yawed circu
(Conditions of Fig. 14)

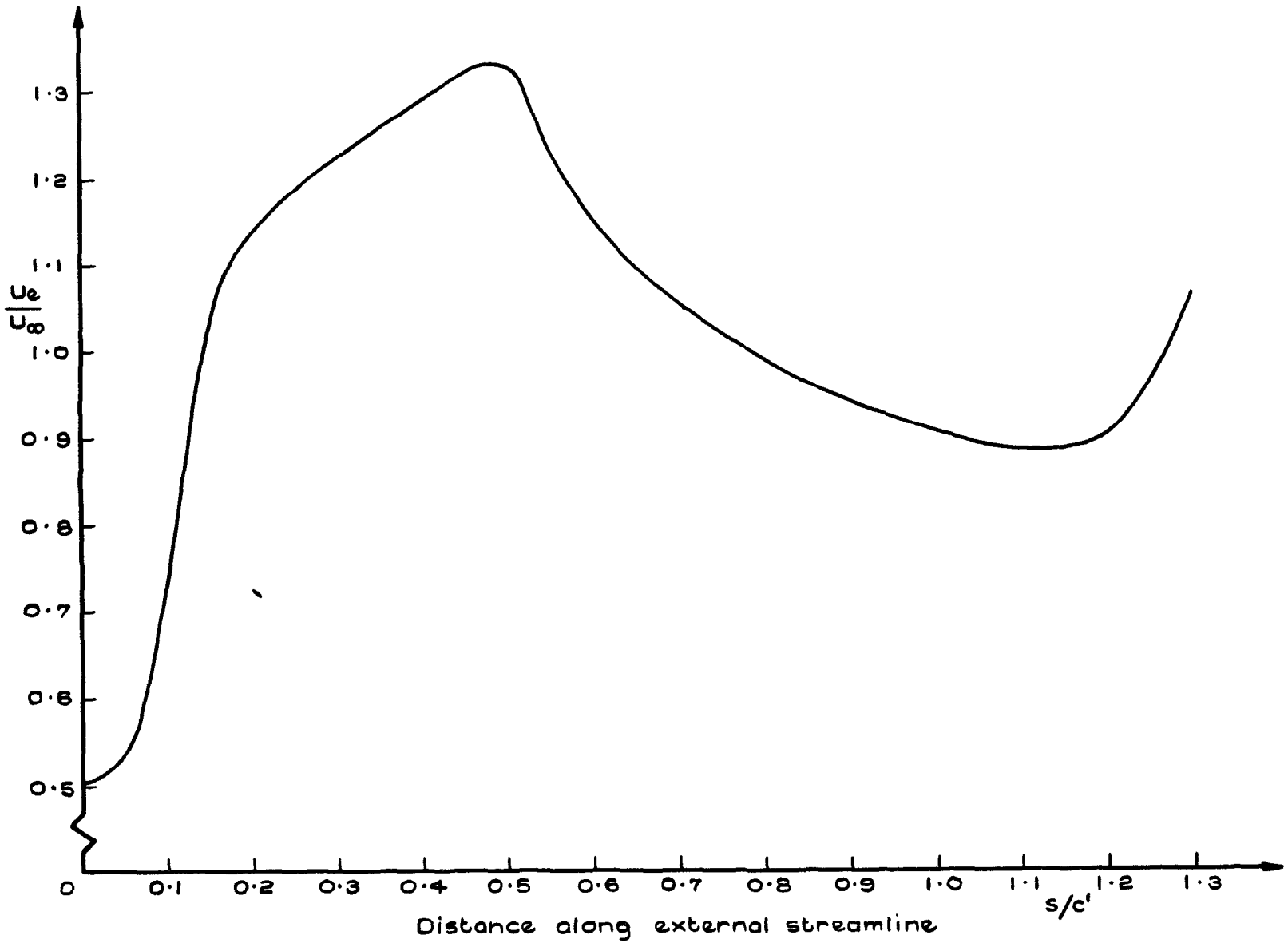

Fig.18 Resultant external velocity distribution for the lower surface of NPL 9510 at $\Lambda = 30^{\circ}$, $M_\infty \cos \Lambda = 0{\cdot}76$

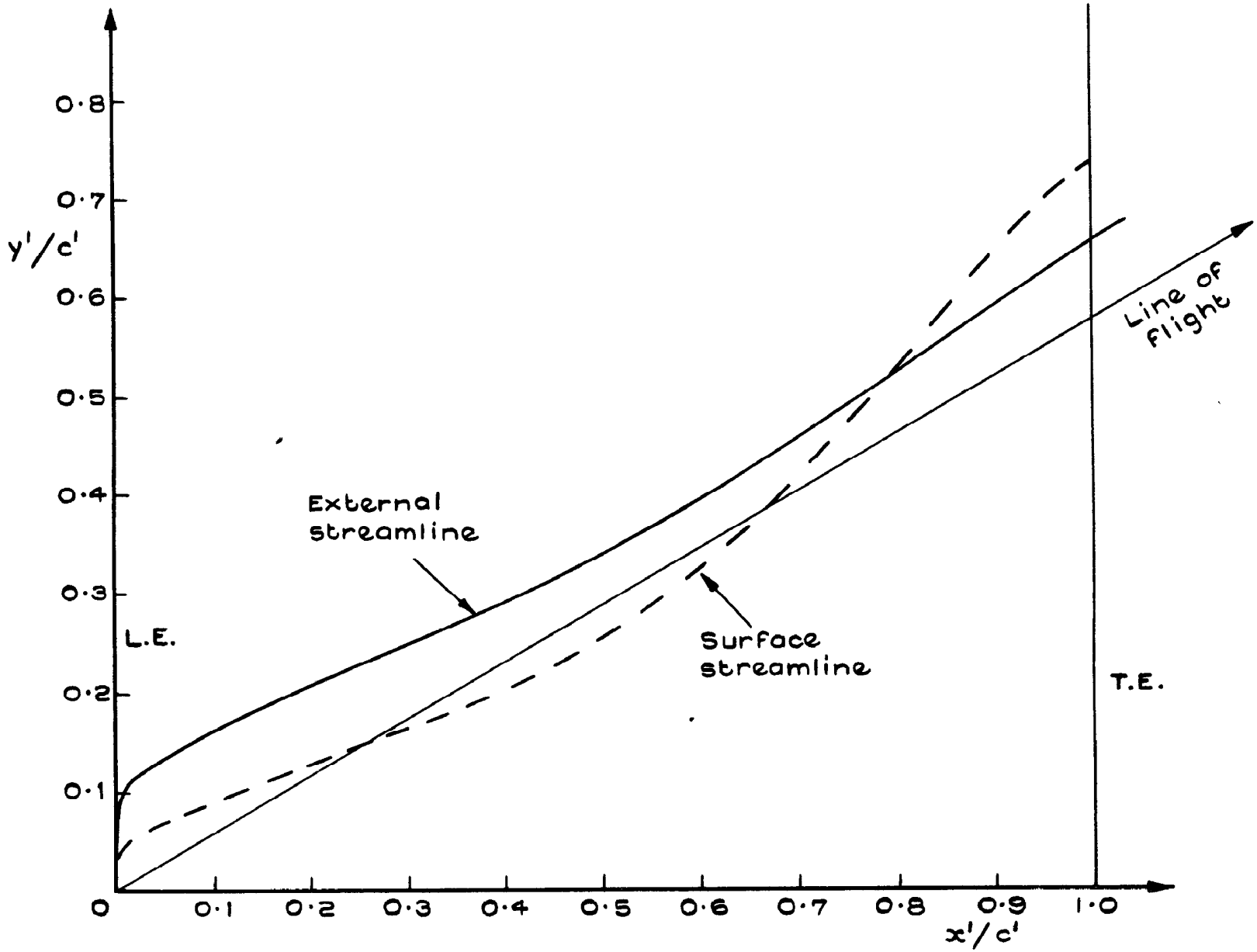

Fig.19 Surface and external streamlines predicted for the lower surface of NPL 9510 at $\Lambda = 30^{\circ}$, $M_{\infty} \cos \Lambda = 0 \cdot 76$

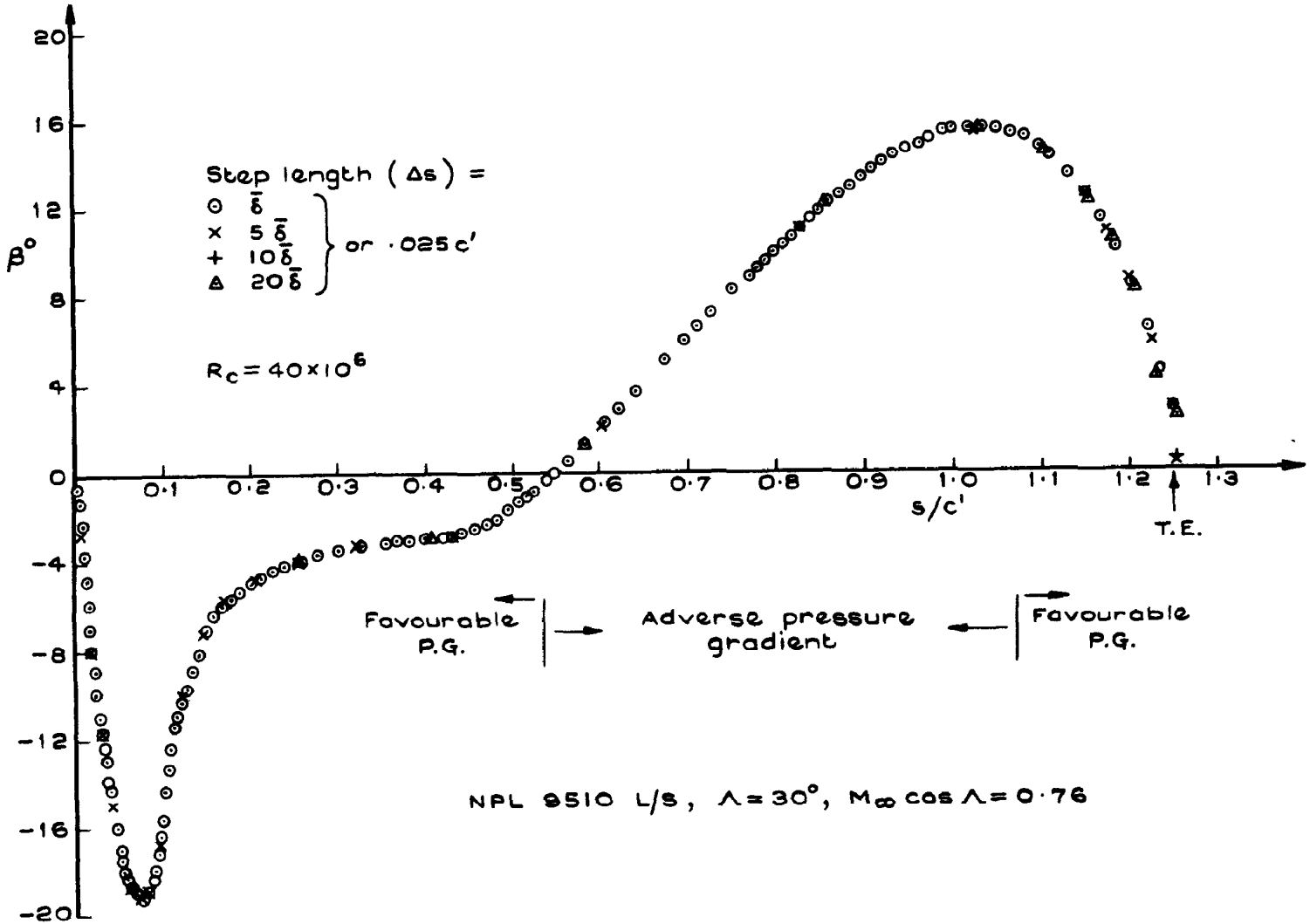

Fig.21 Effect of step size on predictions of present method

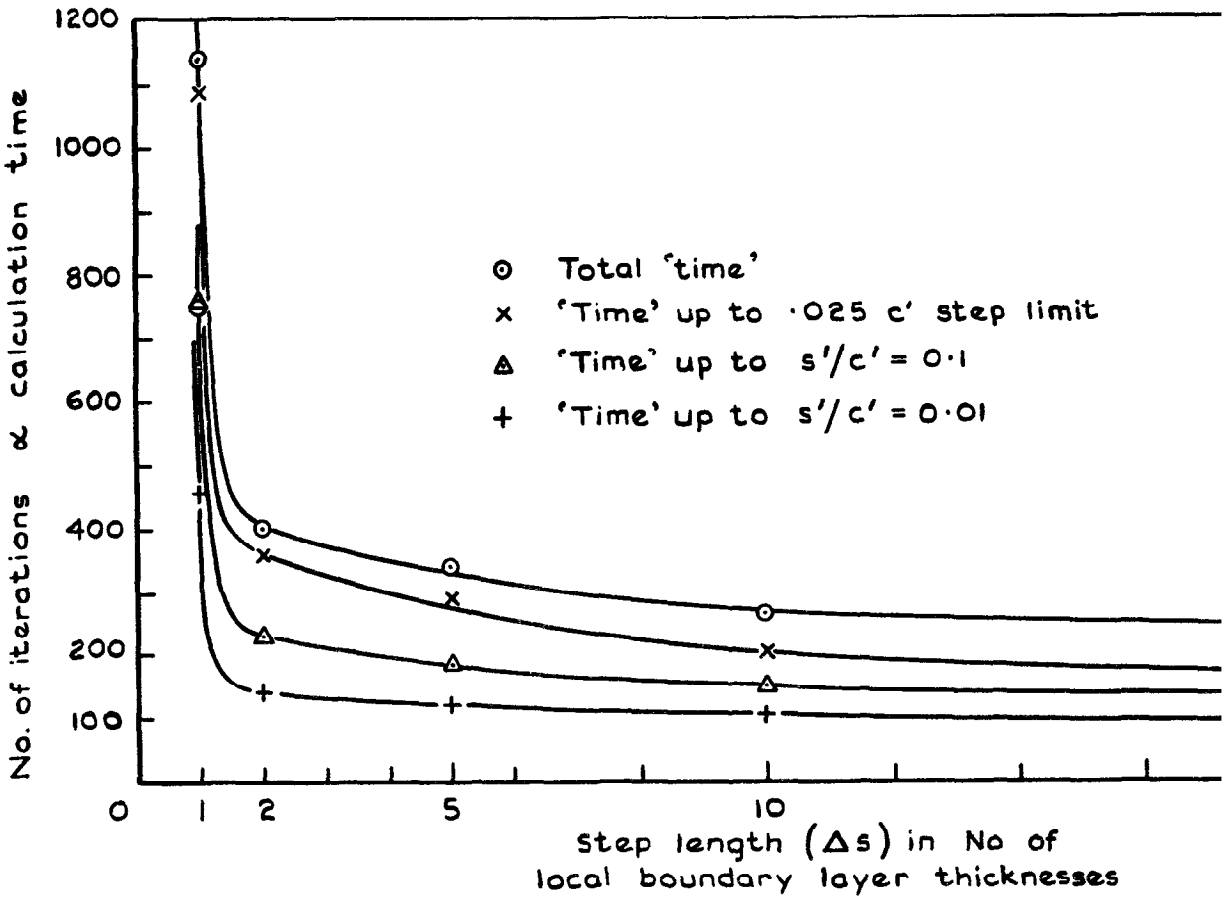

Fig.22 Variation of calculation 'time' with step length for of Figures 18 to 21 (ie NPL 9510 L/S etc)

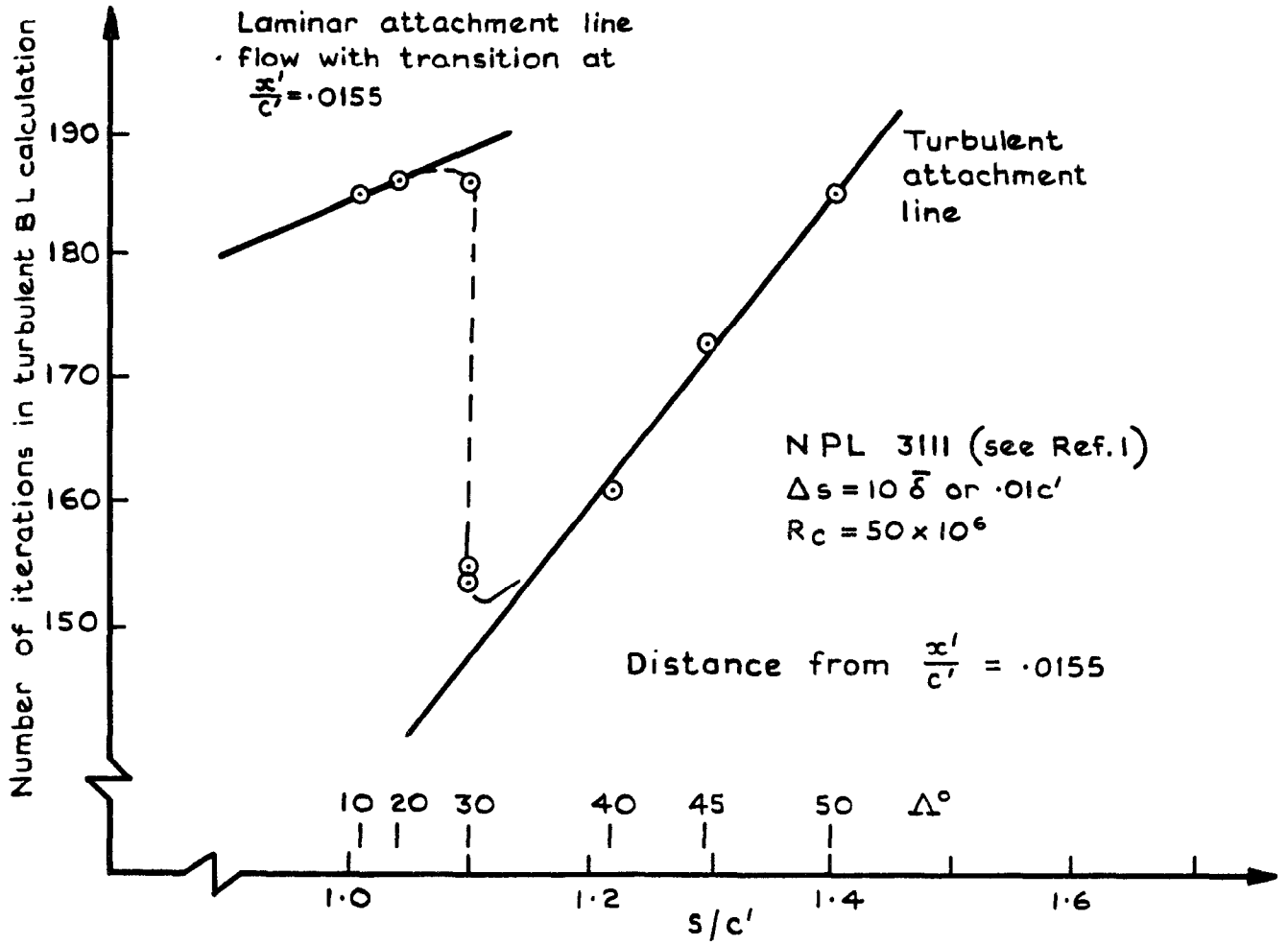

Fig. 23 Variation of calculation 'time' with sweep

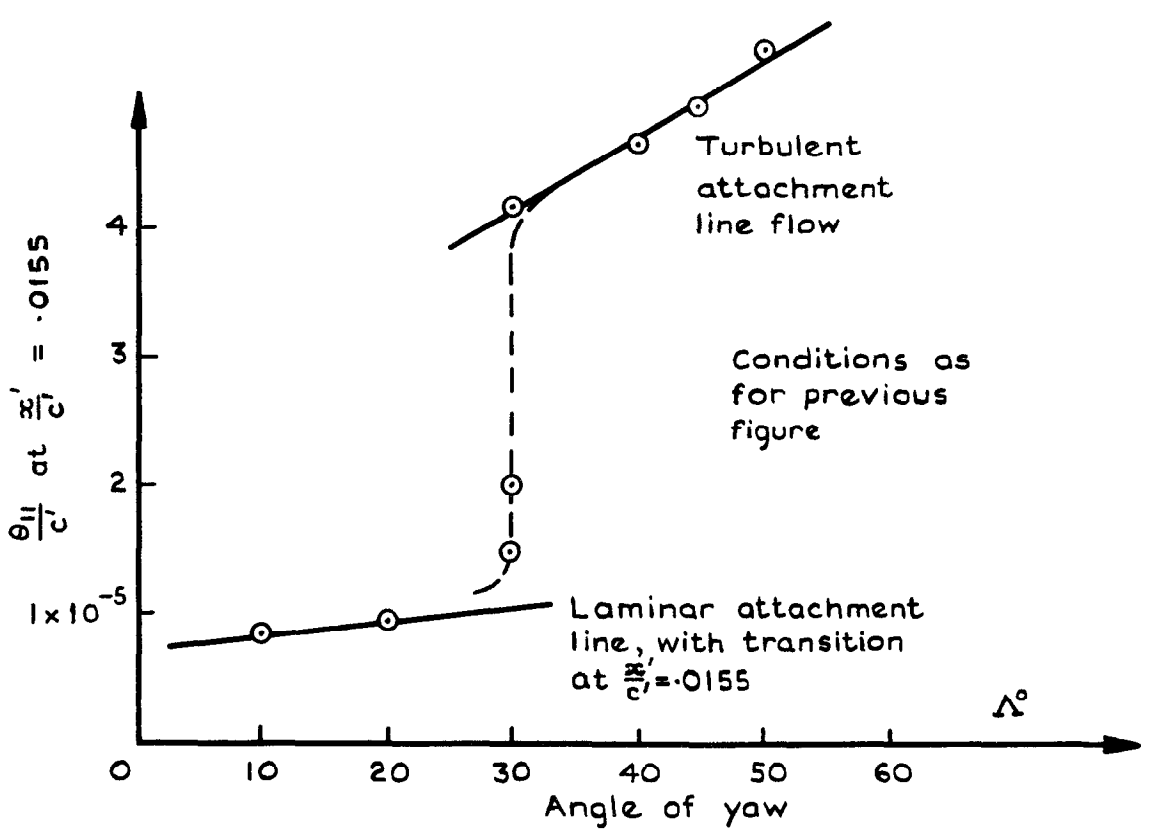

Fig. 24 Performance of present method for parametric study of Ref. 1

Printed in England for Her Majesty's Stationery Office by the Royal Aircraft Establishment, Farnborough. Dd. 505376 K4 11/74.

1974

Published by
HER MAJESTY'S STATIONERY OFFICE

Government Bookshops
49 High Holborn, London WC1V 6HB
13a Castle Street, Edinburgh EH2 3AR
41 The Hayes, Cardiff CF1 1JW
Brazennose Street, Manchester M60 8AS
Southey House, Wine Street, Bristol BS1 2BQ
258 Broad Street, Birmingham B1 2HE
80 Chichester Street, Belfast BT1 4JY
Government Publications are also available through booksellers

C.P. No. 1307

ISBN 011 470891 6